9-22-1990

Thin film adhesion measurement using excimer laser ablation test

Wen-Chieh Lee

Thin Film Adhesion Measurement Using Excimer Laser Ablation Test

by

Wen-Chieh Lee

Thin Film Adhesion Measurement Using Excimer Laser Ablation Test

by

Wen-Chieh Lee

Sept. 22 1990
Date

Thin Film Adhesion Measurement Using Excimer Laser Ablation Test

by

Wen-Chieh Lee

A Thesis Submitted in Partial Fulfillment
of the Requirements for the Degree of

MASTER OF SCIENCE

in Materials Science and Engineering at

The Rochester Institute of Technology

Approved by:

4/8/91

Dr. Vern Lindberg, Thesis Advisor
Physics Department
Rochester Institute of Technology

4/8/91

Dr. Alan B. Entenberg, Faculty Member
Physics Department
Rochester Institute of Technology

Dr. Paul H. Wojciechowski
Kodak Research Labortories
Eastman Kodak Company

CONTENTS

List of Figures

List of Tables

Table page

Acknowledgement

I would like to give my gratitude to Dr. Vern Lindberg, my thesis advisor, who spent an enormous time on guiding and revision of this thesis. Also special thanks for the sponsorship and discussions from Dr. Paul Wojciechowski, who made my research at Kodak research laboratories possible and presented this topic in the second symposium of Electro-Chemical Society in Montreal, May 1990. Thanks to Dr. Frank Duarte for his instrumental help, too.

Dedication

To Li-Chun, father, and mother.

ABSTRACT

An excimer laser incident on a metallic thin film is used to measure the adhesion between the film and the substrate. The initial optical absorption leads to electron excitation. After collisions and degradation of the excited electrons, the absorbed energy is transferred into various kinds of energy among which the major one is thermal. The superheated surface undergoes vapor explosion which serves as one source of shock wave to break the thin film. The evaporated particles may recoil back to the surface constructing another shock wave to break the film. In addition, a tensile stress may be formed by the large difference of thermal expansion between metallic thin film and polymeric substrate. All these effects cooperate to cause the cracking of the metallic thin film.

This thesis provides the theoretical models to explain how the various mechanisms work on adhesion evaluation. Based on these understandings, the experimental data of laser ablation test is more suggestive and meaningful than the tape test which is sometimes ambiguous due to un-discerned effects.

The experimental results show that laser ablation is sensitive to small differences in adhesion. In addition, the laser ablation test has a broader range of measurement as compared to that of tape test. One thing to be noticed is that laser ablation test is strongly affected by the thickness of the film.

1. INTRODUCTION

1.1 Adhesion of Thin Films: Definition and Importance

The nature of the interface between a thin film and a substrate is of critical importance to the performance of the combination. Among the various characteristics of the interface, an essential criterion for applicability of the thin film is the durability of the film-to-substrate interface. In this respect, adhesion is of the prime importance.

The word adhesion is frequently used in a broad sense to describe the sticking together of two materials. Actually it describes a complex combination of mutual attraction and mechanical interlocking of two materials. (Mittal et al defined four mechanisms of adhesion, see Reference 1.)

According to Van der Waal's effect, the total attractive energy of two non-polar atoms or molecules is expressed as

$$U = -\frac{h(\upsilon_1 \upsilon_2)}{\upsilon_1 + \upsilon_2}\frac{\alpha_1 \alpha_2}{r^6} \qquad (1.1)$$

where h is Plank's constant, υ_1 and υ_2 are atomic oscillation frequencies, α_1 and α_2 are polarizabilities, and r is the atomic separation.

For dipolar molecules, the attractive energy can be expressed as:

$$U \approx -\frac{h(u_1 u_2)}{u_1 + u_2}\frac{1}{r^6}\frac{1}{kT} \qquad (1.2)$$

where u is molecular dipole moment and k is Boltzmann's constant.

For induced polarized molecules, the attractive energy can be expressed as:

$$U = -(\alpha_1 U_2^2 + \alpha_2 U_1^2)\frac{1}{r^6} \qquad (1.3)$$

where u_1 and u_2 are molecular dipole moments.

All three kinds of attraction are inversely proportional to the sixth power of atomic separation and are very powerful over short distances.

Mechanical interlocking of film and substrate is shown in Figure 1.1. When the film is detached from the substrate, not only the interfacial bonding (A) but also the intrinsic bonding (B and C) are to be broken (Reference 17). Therefore the measured energy to separate the two materials is actually a complex combination of interfacial bonding and intrinsic bonding.

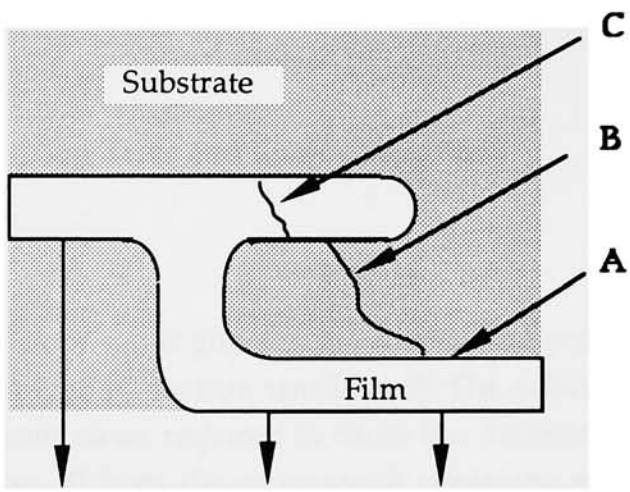

Figure 1.1 Mechanical Interlocking of two materials. A Type bonding is interfacial bonding. B and C type bondings are intrinsic bondings.

Traditional techniques, such as peel and scratch tests, used to evaluate film-to-substrate adhesion are mainly done by breaking film-to-substrate systems mechanically. In these tests, the energy or force required to initiate a certain type of damage on the system is correlated with the adhesion property (Reference 27). While these methods can provide quantitative and qualitative informations, as was stated by Mittal et al (Reference1), no engineering test is able to directly reveal the basic adhesion, i.e., the interfacial bonding strength. The main reason is that the mode of deformation caused by traditional tests is

a complex combination of elastic, plastic and brittle deformations. One can hardly know the role of a specific mechanism in the total deformation. Therefore traditional mechanical tests may be insensitive to the small changes in adhesion.

However, the sensitivity to basic adhesion of a testing technique is always desirable because our main method to improve the adhesion is to modify the bonding state at the interface rather than to improve the mechanical interlocking.

An advantage of the laser ablation test over traditional ones is its sensitivity to small adhesion differences. The failure mechanism can also be modeled theoretically and therefore has the potential to evaluate adhesion both quantitatively and qualitatively. The testing of a sample is relatively quick and does not require special sample preparation.

1.2 Traditional Adhesion Tests and Their Limitations

1.2.1 Pull-Off Test

In this test a tape or rod is glued to the coating and pulled off by a normal tensile stress (e.g. by Instron tensile test). The adhesion is measured either by the minimum stress required to cause the detachment or by the area of the thin film taken off from the substrate. A schematic presentation of this test is shown in Figure 1.2 .

A main drawback of this technique is that comparison of the results acquired by using different glues is very difficult. Besides, for porous films the bonding agent may diffuse through the coating which produces non-uniform tensile stress on the system.

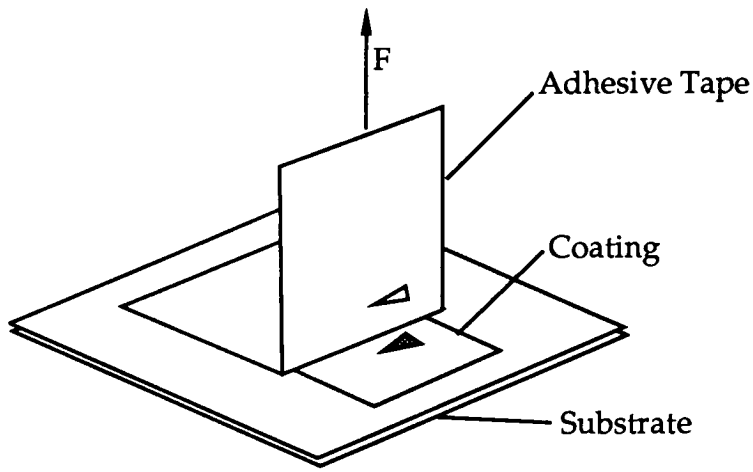

Characterisctics: Removed area, Peeling Energy

Figure 1.2 Schematic presentation of peel-off test.

1.2.2. Scratch test

In this test a scratching point is drawn across a coated sample. Figure 1.3 shows this technique schematically. The scratching point produces an elastoplastic deformation on the film-to-substrate system. The minimum load at which the system failure occurs, the critical load, is used to measure adhesion. This testing method can be coupled with acoustic emission monitoring in order to improve the sensitivity. During this revised process, the acoustic transducer reveals the noise generated from the system. The noise level of the acoustic signal corresponds to various kinds of bond breaking processes. Upon the breaking of the interfacial bonding which corresponds to the adhesion condition of the system, a unique signal level (compared to the one with no interfacial bond breaking process) will appear. We thus can utilize the minimum load to initiate this unique noise level to characterize the adhesion condition of the system. A drawback of this test is that the results for coatings on soft substrates includes the deformation of substrate as well as adhesion and these can not be separated easily. Determination of the critical load is also difficult because the coating material may flow under the stylus which reduces the usefulness of the test.

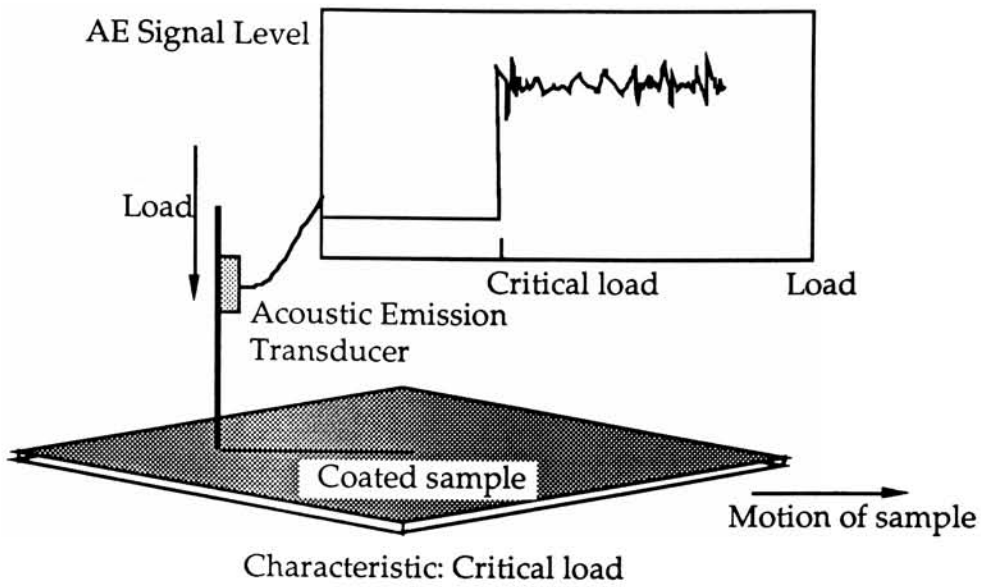

Figure 1.3 A schematic presentation of scratch test. A sample is pulled from under a stylus while the load is increased. Critical load for adhesion failure is accompanied by acoustic emission.

1.2.3. Ultracentrifugal test

In this test a cylindrical substrate is coated by a thin film and is rotated at an increasing speed until the coating is detached from the substrate. An alternative method is to glue a coated substrate to the wall of the cylinder. Figure 1.4 shows this test schematically.

The adhesion property of the system is characterized by

$$F/A = 4\pi^2 N^2 r \rho d - \rho d / r \qquad (1.4)$$

where F is the ultracentrifugal force required to detach the film, A is the area of the detached coating, N is revolutionary rate (revolutions/sec), r is the radius of the cylinder, ρ is the density of the film, and d is the thickness of the film.

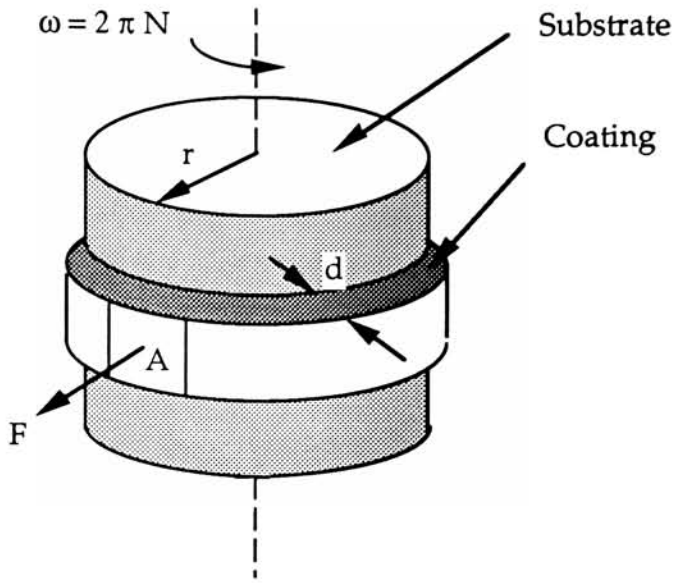

Figure 1. 4 Ultracentrifugal test

The main drawback of this test is that sometimes the adhesion is stronger than the resistance of the glue so that the glue fails before the interface does. In this case, the data yielded by this method actually is the durability of the glue rather than the adhesion of the system.

Because all of these tests are not directly correlated with fundamental adhesion, comparison between the data acquired by different testing techniques is difficult.

The advantage of the laser ablation test over the other tests is that its failure mechanism is more explainable than the other tests. The quick processability, wide range of adhesion measurement and high sensitivity allow us to understand the adhesion property more efficiently.

1.3 Laser Ablation Test

1.3.1 History of Preliminary Results

In 1970, Nordin C. Anderholm and Albert Goodman (Reference 3) suggested an application of laser light to thin film adhesion measurement. According to their suggestions, a compressive stress wave was generated by an

adiabatic explosion of a metallic absorbing material, and when the compressive stress wave traveled through the film-to-substrate interface, a portion of it was reflected into tensile form. This is shown in Figure 1.5. If the magnitude of this tensile stress were greater than a certain threshold value, interfacial failure occured. Such an interfacial failure was correlated with the adhering property of the film-to-substrate system. Hence the adhesion of a system was characterized by the threshold energy density required to break the thin film.

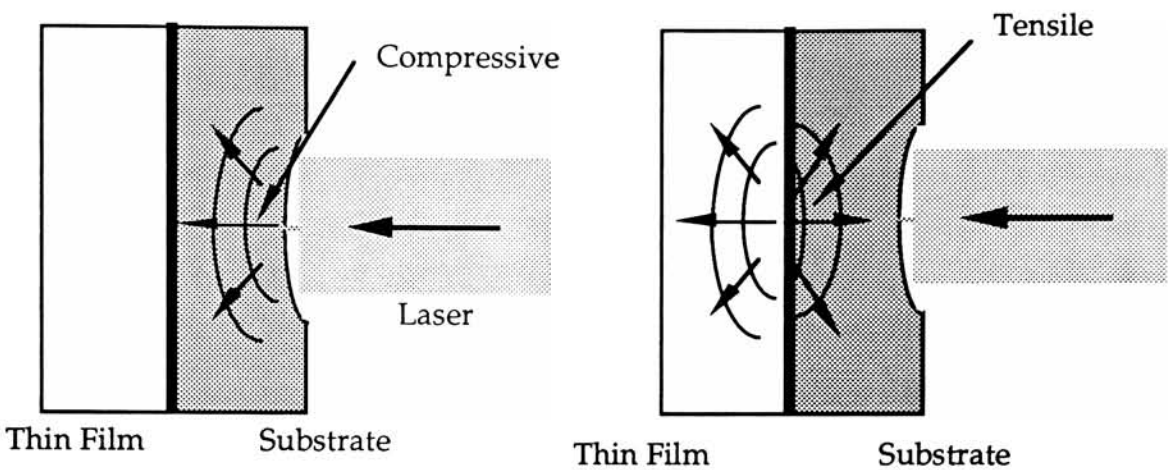

(a) A compressive stress wave is generated by laser light

(b) A tensile stress wave is reflected from the interface

Figure 1.5 The generation of tensile stress by laser light.

In 1987, J. L. Vossen (Reference 2) used this method for metallic thin films deposited on SiO_2. In his test, the thin film was patterned into small dots with diameter less than that of the laser beam cross section. As is shown in Figure 1.7(a), an absorbent layer was coated on the back side of the substrate and was hit by laser light of wavelength 1.06 μm. According to Vossen, the required energy density to break the thin film was higher for a better adhering system than for a poorer adhering system. Results are shown in Figure 1.6. Therefore, the laser ablation test could be an alternative means to measure adhesion. Vossen's test worked well for hard substrates, but due to strong damping in a polymeric substrate, his method was not suitable for metal/polymer systems.

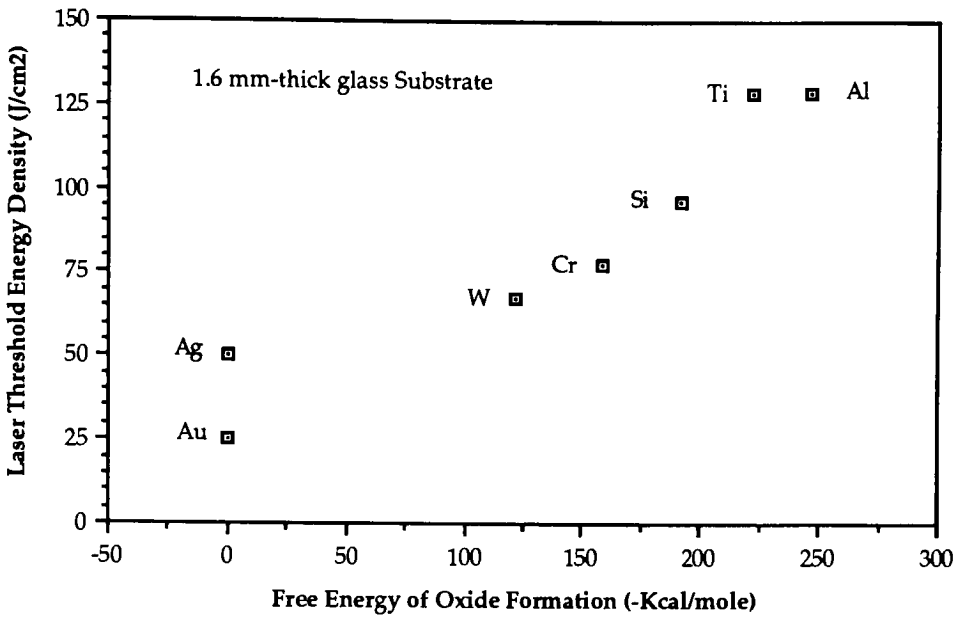

Figure 1.6 Spallation threshold for various metal films deposited on fused silica substrate. (Reference 2)

In 1988, P. H. Wojciechowski, F. J. Duarte, and A. L. Hrycin (Reference 4) reported the result of impinging laser light directly on a silver thin film coated on a polymer (Ag/polyethylene terephthalate (PET), see Table 1.1). Figure 1.7 shows this experimental set-up.

In their test, a rectangular laser beam,12x25 mm, was focused by a lens. The energy density of beam along the shorter side was Gaussian, while along the longer one it was roughly constant. Due to the convergence of the laser beam caused by lens, the incident energy density (energy per unit area) of laser light increased as the distance from the sample to focus decreased. When the incident energy density exceeded a threshold value, a crack was seen on thin film. Dividing the incident energy by the measured area of the evaporated pool on thin film yielded the threshold energy density for cracking the thin film.

Wojciechowski compared the threshold intensities between a sample that had been ion bombarded before deposition and the non-bombarded ones.

The ion bombardment had been empirically known able to enhance the adhesion. This was authenticated by Wojciechowski's tests—higher threshold energy density for ion bombarded samples than for non bombarded ones. Results are in Table 1.1.

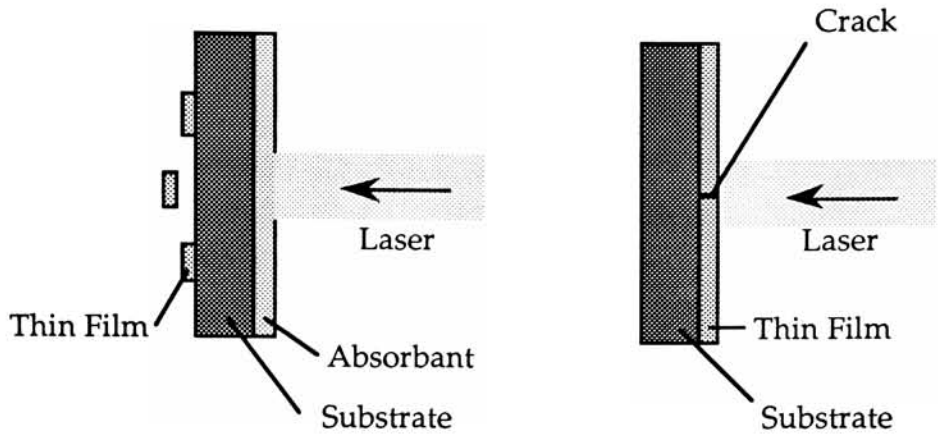

(a) Vossen's Method

(b) Method used in this thesis research

Figure 1. 7 (a) J. L. Vossen's Adhesion tests. (Reference 2). (b) this thesis' test (same as P. H. Wojciechowski's, Reference 4).

Table 1.1 Adhesion Test of Silver on PET

Film : Ag, Substrate: PET, Laser Beam : XeCl Excimer Laser (308 nm)			
#	**Ion Bombard**	**Tape Test**	**Laser Threshold Energy Density**
1	Y	No	424 mJ/cm^2
2	N	No	303
3	N	No	303
4	N	No	333

Because this method saves the inconvenience of preparing double sided coating, it definitely enhanced its applicability as compared to Vossen's test, although the failure mechanism was not known.

The objective of this thesis research is to model the failure mechanism and confirm the conclusions made by Wojciechowski.

1.3.2 Laser ablation test in this thesis research

In this thesis research, the light source, samples, and experimental methods are virtually the same as Wojciechowski's (details are in experimental section). The main difference is that the surface treatment adopted for improving adhesion was oxygen glow discharge instead of ion bombardment. According to our knowledge (see Section 3.3 group 2), oxygen glow treatment improves the adhesion between the thin film and the substrate by providing more radicals on the polymer surface which are attractive to the metallic thin film. Thus the threshold energy density of laser light to crack the thin film coated on glow treated substrate is supposed to be higher higher than that of non-glow treated ones.

2. THEORY

2.1 Overview of Interaction of a Laser Pulse with Matter

Laser light, in order to cause any lasting effect on a material, must first be absorbed. The subsequent effects, including thermal, chemical, and mechanical, are generated by the absorbed energy. Therefore it is this "secondary source", the absorbed energy, that determines what happens to the irradiated material.

Upon the impact of a laser beam on a material, electromagnetic (EM) energy is converted first into electronic excitation. After a short period of degradation and collision of electrons, the absorbed energy is then converted into various kinds of energies which in turn assist the removal of the materials by various mechanisms. In most cases, the removal of the laser irradiated materials can be well controlled by putting some chemical reactive species i.e. Cl_2 and CF_3Br which involve extensive heating, binding, and eventually evaporating in the so called laser etching process. However, the removal of the materials can also occur without the use of reactive intermediate species. In these cases, materials actually dissociate by rapid evaporation which is called "laser ablation". From the view of physics, laser ablation occurs when a large amount of electronic excitation energy is transferred into molecular or atomic vibrational energy; for non-ablative effects, more energy is transferred into chemical energy than into mechanical energy. (References 5,10,11,12).

The initial conversion, electronic excitation, has little direct effect on adhesion since the absorption depth, typically tens of nm for ultraviolet (UV) light on metal, is much smaller than the thickness of the film which is thicker than two hundred nm in our samples. The preceeding thermal conversion will lead to melting and evaporation at the surface of the thin film. For the metal/polymer system, both the film and substrate suffer from the heat generated by the laser light. Because the softening temperature of polymer (T_g < 300 K) is much lower than that of metal, the polymer at

interface can be molten prior to the metallic film reaches its melting point. In such a case, there will be a thin liquid layer at the interface. In addition to the melting effect caused by heat, a thermal stress due to the large difference in thermal expansion of the polymer and the metal is generated at the interface. Such a thermal stress serves as one source for cracking thin films.

When the superheated materials evaporate into the air, a shock wave is generated by a vapor explosion. This shock wave serves as one source of stress for cracking the thin films, too.

The evaporated metal film may form a layer of plasma known as the Knudsen layer above the surface. Within such a Knudsen layer, some of the particles recoil back to the laser impinged area with very high speed producing a shock wave on the material. This shock wave also serves as the third source of stress for cracking the thin films.

In this section, we start from the fundamental theories of laser absorption and then move into the energy conversions. Finally, we suggest a model to explain what we observed in our laser ablation test.

2.2 Absorption and Reflection of Laser Light

When photons hit the target, various kinds of electronic excitations happen. The role of each excitation mechanism depends on the wavelength of the incident light. For UV light, the optical excitation only happens for the outer subshell electrons while X-ray excitation occurs for core electrons.

The strongest excitation removes the electrons from the valence band to the conduction band thus changing the density of free electrons within the material. Accompanying this phenomenon are some minor effects caused by the coupling of electrons, internal magnetic fields, external magnetic field, and electrical field. The two strongest minor effects are (References 6, 13,14,15,16,18):

1. The residual Coulomb interaction, an electrical interaction that happens between all active electrons.

2. The spin-orbit interaction, a magnetic interaction that couples the spin angular momentum of each optically active electron with its own orbital angular momentum.

After being illuminated, the excited electrons may return to lower energy orbits with the extra energy being converted into either photons or phonons. The preceeding absorption process can be thought of as one that gains energy from a "secondary" source of energy inside the material (References 5,19, 20, 21).

The index of refraction, n, is complex :

$$n = n_1 - i\, n_2 \qquad (2.1)$$

where the real part is $n_1 = c/v$, the ratio of the speed of light in vacuum to the speed in the medium, and the imaginary part n_2 gives the absorption coefficient α by

$$\alpha = 4 \pi n_2/\lambda \qquad (2.2)$$

where λ is the wavelength of incident light.

At normal angle of incidence, the reflection coefficient is expressed as

$$R = \frac{I_r}{I_i} = \left| \frac{(n-1)}{(n+1)} \right|^2 \qquad (2.3)$$

where I_i and I_r are the incident and reflected intensities.

The absorption depth is the inverse of α . Since our film is opaque to the laser light (because $1/\alpha$ is much smaller than the film thickness), the absorbance can be expressed as A=1 - R.

Equation 2.4 shows that the absorption coefficient changes with wavelength. Hence the relationship between dielectric constant of material and the wavelength of light is critical to the characteristics of absorption.

For non-magnetic and isotropic material, the dielectric constant and index of refraction are related by

$$\begin{aligned} n^2 &= \varepsilon_1 - i\,\varepsilon_2 \\ &= \varepsilon \end{aligned} \qquad (2.4)$$

where ε is the complex dielectric constant of material.

The real and imaginary parts of n and ε are related by

$$\varepsilon_1 = n_1^2 + n_2^2 \qquad (2.5)$$

$$\varepsilon_2 = 2\, n_1\, n_2 \qquad (2.6)$$

The dielectric constant changes with wavelength. It may also change when the intensity of laser light is high due to spin-orbit coupling changes (i.e. from LS to JJ type). While in this thesis research we don't consider the coupling mechanism, these characteristics do lead to the variation of absorption by metallic materials of different light which is preliminary to the determination of absorbed energy. A detailed discussion is in Section 2.3.

2.3 Absorption of Laser Light by Metals

The optical absorbance of a metal is dominated by its conduction electrons. These free electrons are different from the inner core electrons in that they don't oscillate within the atom and thereby have no resonance frequency. Instead, they behave like a plasma having the plasma frequency ω_p within the material. From quantum mechanics, we have dielectric constant for metal written as (Reference 5)

$$\varepsilon = 1 + \omega_p^2\,(-\tau_e^2 + i\,\tau_e/\omega)(1 + \omega^2\tau_e^2) \qquad (2.7)$$

where ω_p is the plasma frequency

$$\omega_p = (N_e e^2/m_e \varepsilon_0)^{1/2} \qquad (2.8)$$

τ_e is the collision time of electrons, N_e is the number density of free electrons within the material, and ω is the angular frequency of the light.

At $\omega = \omega_p$, in the ultraviolet for metals, the optical properties are rather different above and below the plasma frequency. This leads to large R and α for $\omega < \omega_p$ and small R and α for $\omega > \omega_p$.

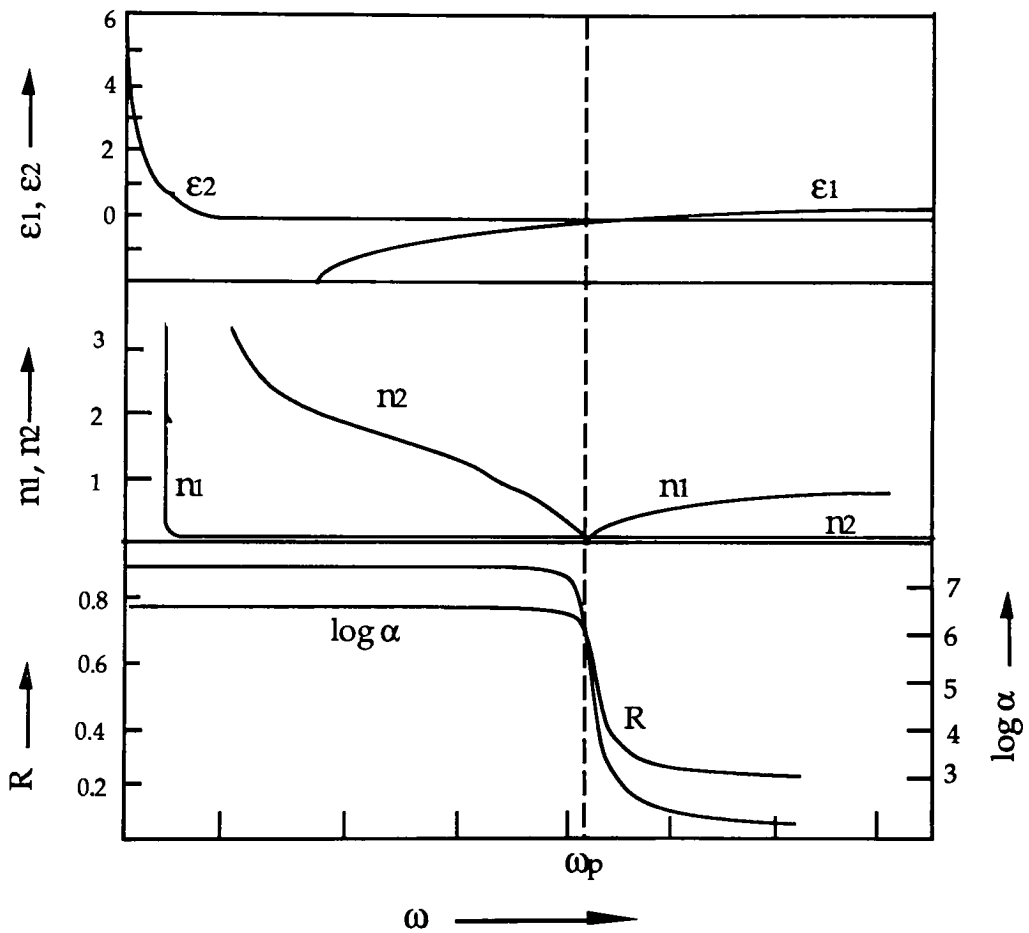

Figure 2.1 The frequency dependence of metals. (Figure is transcribed from Reference 5, in which the data are calculated for $h\omega_p = 8.3$ eV, corresponding to $N_e = 5 \times 10^{22}$ cm^{-3}, $h/\tau_e = 0.02$ eV)

Figure 2.1 shows the frequency dependence of the dielectric constant of metals.

Table 2.1 a Spectrophotometric data for Ag thin film (2000 Å).

Wavelength (nm)	Absorbance (%)	Transmittance(%)
300	85.1	0.0
302	86.5	0.0
304	88.2	0.0
306	89.2	0.0
308	91.0	0.0
310	92.5	0.0
312	93.9	0.0
314	95.1	0.0
316	96.1	0.0
318	96.8	0.0
320	96.7	0.0

The optical properties of a free electron metal in the region $\omega < \omega_p$ are related to its DC conductivity, σ_0, which can be expressed as

$$\sigma_0 = \omega_p^2 \varepsilon_0 \tau_e \qquad (2.9)$$

Values of α and R in two spectral regions can be expressed as:

A. In the far infrared region:

$$1 - R = (8 \varepsilon_0 \omega/\sigma_0)^{1/2} \qquad (2.10)$$

$$\alpha = (2 \omega \sigma_0/\varepsilon_0 c^2)^{1/2} \qquad (2.11)$$

B. In the near infrared to ultraviolet region:

$$1 - R = 2\,\varepsilon_0\,\omega_p/\sigma_0 \tag{2.12}$$

$$\alpha = 2\,\omega_p\,/c \tag{2.13}$$

Besides the relation shown above, one other consideration is to be taken into account when the material is illuminated by UV, the interband transitions. The d-electrons make a bound-type contribution to the dielectric function, and since the contribution to ε_1 is positive, the point $\varepsilon_1 = 0$ which defines ω_p is shifted to a lower frequency. Figure 2.2 shows this effect.

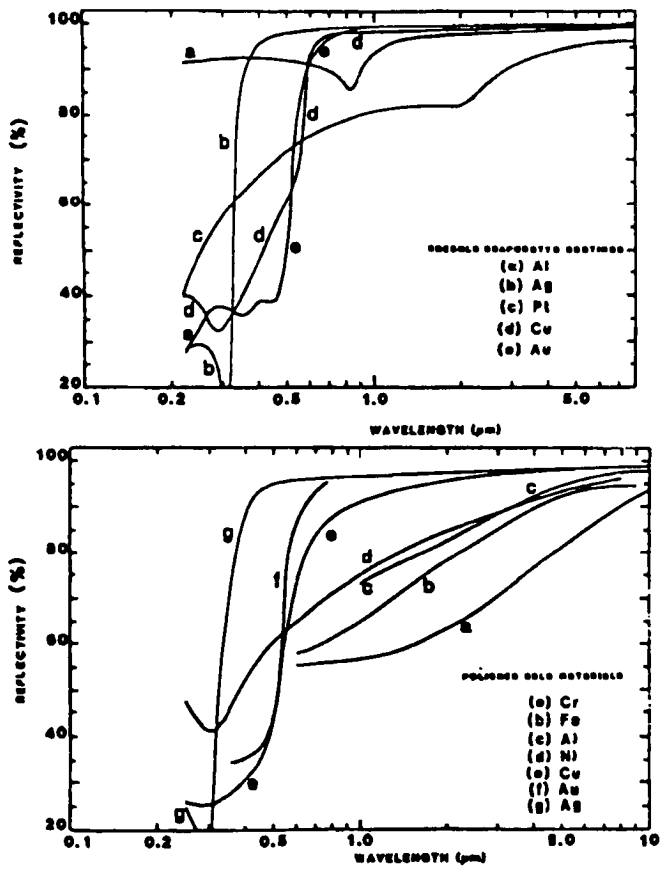

Figure 2.2 Optical reflectivity of selected metals is shown as a function of wavelength for freshly evaporated thin films. (Reference 5)

As seen in Table 2.1, the transmittance of UV light by silver is very small. Thus, given the incident energy density dE/dÆ (dE is the net absorbed energy and dÆ is laser impinged area) and the absorbance A, we can determine the absorbed energy density (E) as

$$dE/d\text{Æ} = E\,(1\text{-}R)\,/\text{Æ} \qquad (2.14)$$

2.4 Conversion of Energy Subsequent to Absorption

2.4.1 Overview of Subsequent effects

The degradation of ordered and localized primary excitation energy into uniform heat involves three steps. First, the locally excited electrons must be spatially distributed by temporal randomization in the collision time. (This time is shorter than an optical cycle so that we deem it as a simultaneous effect with the laser irradiation). Next the energy is transferred to the surrounding atoms by electron-atom and electron-electron collisions. We characterize this thermal effect by an overall relaxation time, τ_E (different from electron collision time), for the excited materials to return to the ground state. This is about 10^{-13} s in a metal. The last step is heat flow and evaporation. For thin films we concentrate on the last effects.

Several articles discuss the effects subsequent to laser irradiation (References 22-46). We will only concentrate on the stress that generates a crack on a thin film by three major means: vapor explosion (Reference 33), recoil pressure from the Knudsen layer, and thermal expansion (Reference 40). The following paragraph is to explain how these resources are used to measure adhesion. Morphological changes subsequent to thermal diffusion are also to be discussed.

2.4.2 Vapor explosion phenomenon

Due to the very short pulse duration (20 ns) in our test, the laser irradiated area on thin film is adiabatically superheated. The superheated material tends to boil in a short time hence generates a vapor explosion by the

rapid nucleation rate of vapor bubbles. The rate of steady-state homogeneous vapor nucleation rate Y(T) (atoms/unit volume) is expressed as

$$Y(T) = A N \upsilon_j \exp(-\Delta g_N/kT) \qquad (2.15)$$

where A is a constant, N is the number of atoms per unit volume, υ_j is the atomic oscillation frequency, Δg_N is the free energy for forming a critical vapor nucleus, k is Plank's constant, and T is temperature in Kelvin (Reference 5).

Because the oscillation frequency is correlated with temperature by

$$h\upsilon = \tfrac{3}{2}kT \qquad (2.16)$$

the bubble nucleation rate can be re-expressed as

$$Y(T) = A N \tfrac{3}{2h}kT \exp(-\Delta g_N/kT) \qquad (2.17)$$

As Equation 2.17 shows, the nucleation rate increases dramatically as the temperature increases. This phenomenon suggests that the the shock wave caused by vapor explosion can be so large that it may serves as a source of stress for cracking the thin film.

2.4.3 The Knudsen layer and ablation pressure

The evaporated particles escaping from the hot surface have a Maxwellian distribution corresponding to the surface temperature, but their velocities are all directed away from the surface. Thus the particles have a velocity component perpendicular to the surface that is much larger than the other two components parallel to the surface. After a few mean free paths (typically a few μm), the velocity distribution returns to isotropic by collisions among particles. Such a region above the evaporating surface is called a Knudsen layer. Some particles experience large angle collisions and scatter back to the surface with very high speed. It is these scattered particles that

construct a very high ablative pressure (of GPa magnitude for aluminum illuminated by UV laser light of 10^{12} W/cm^2) at the surface. If the surface temperature is below the boiling point, we may apply the knowledge of vapor pressure and statistical mechanics to derive recoil pressure. The actual pressure P_d is:

$$P_d = (1+\gamma)\, P_v = 0.54\, P(T_0) \qquad (2.18)$$

where P_v is the pressure just beyond the Knudsen layer, T_0 is the temperature at the dense phase (the surface), and γ is the adiabatic index of the vapor, 5/3 for monoatomic ideal gas.

A simple way to visualize this process is to think of the evaporating surface as a piston that exerts a pressure P_d onto the material. Figure 2.3 shows this and Figure 2.4 shows the distributions of velocity, density, and pressure within the Knudsen Layer.

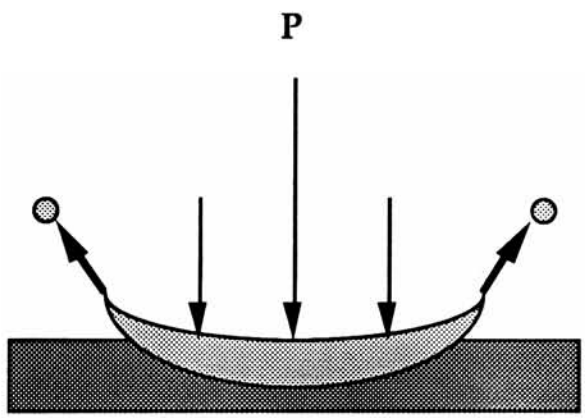

Figure 2.3 Piston mechanism of the evaporating recoil pressure.

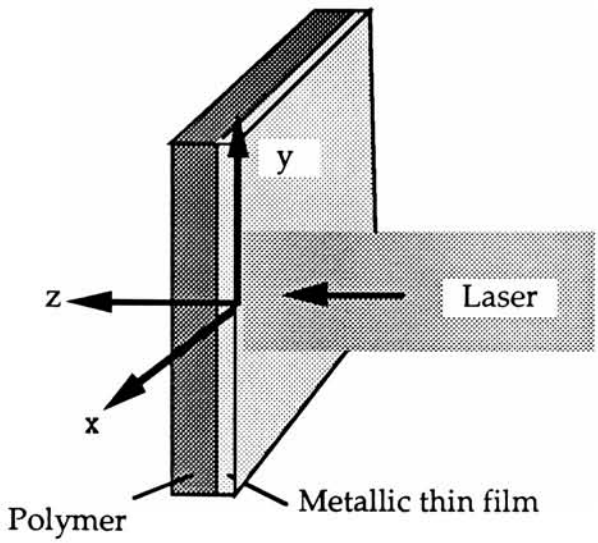

Figure 2.4 a) Coordinate system.

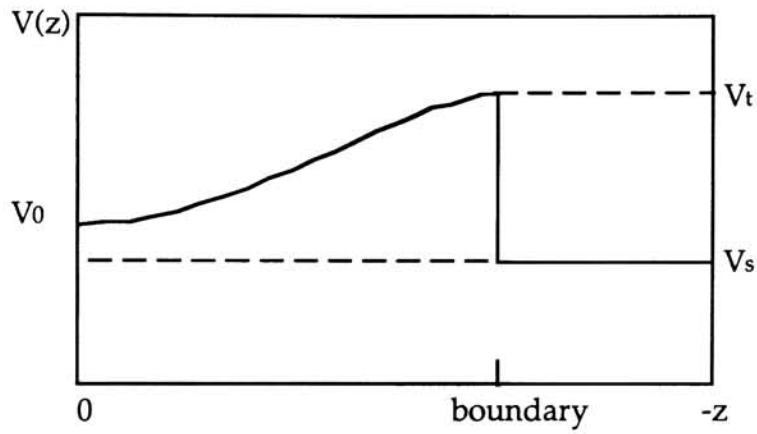

Figure 2.4 b) Distribution of velocity within Knudsen layer. For all codes in Figure 2.4, o refers to surface, t refers to peak, and s refers to beyond the boundary of Knudsen layer. At the surface of thin film, z=0. (Reference 7)

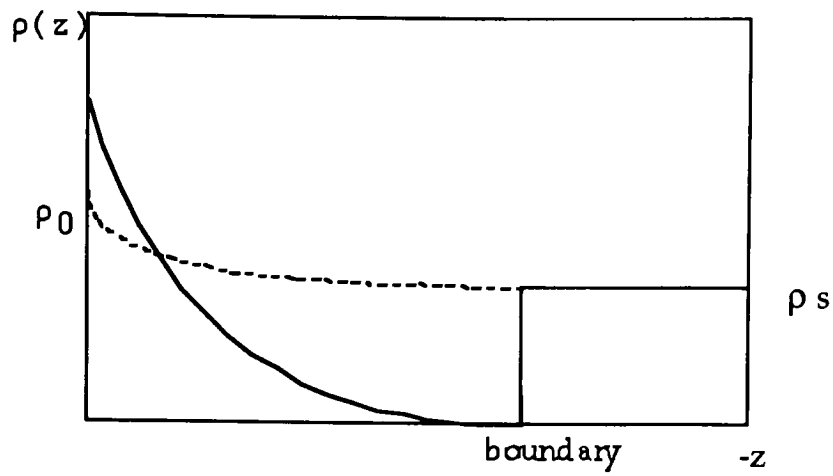

Figure 2.4 c) Distribution of density within Knudsen layer. (Reference7)

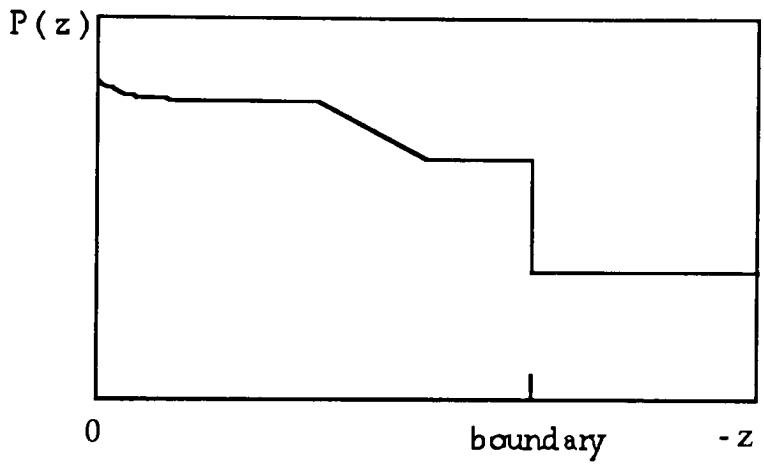

Figure 2.4 d) Distribution of pressure within Knudsen layer.

The vapor can be considered as an ideal gas due to very high temperature, thus the velocity of the evaporated particles follows a Maxwellian distribution in the vicinity of evaporating surface and due to the recoil phenomenon a discontinuity of distribution exists at the boundary of Knudsen layer. Based on this understanding and the profile shown in Figure 2.4b, we depict the distribution of particles as

$$f(-z, v) = \delta(-z)\, f_1(v) + [\, 1 - \delta(-z)\,]\, f_2(v)$$

where

$$f_1(v) = n_0\left(\frac{m}{2\pi kT_0}\right)^{3/2}\exp\left(-mv^2/2kT_0\right), \qquad vz>0$$

$$= \beta f_2(v), \qquad vz<0$$

$$f_2(v) = n_1\left(\frac{m}{2\pi kT_1}\right)^{3/2}\exp\left[-m((v_z-u_1)^2+v_x^2+v_y^2)/2kT_1\right]$$

$$u_1^2 = \sqrt{kT_1/m}$$

δ (-z) is an unknown function that satisfies the conditions $\delta(0) = 1$ and $\delta(- z =$ boundary) $= 0$, T_0 is metal surface temperature, and n_0 is the saturated density of vapor at this temperature. T_1, n_1, and u_1 refer to the state beyond the discontinuity. When there is no atmosphere around the evaporated particles and the explosion occurrs adiabatically, we have

$$\beta = 6.29,\ T_1=0.67\ T_0,\ \text{and}\ n_1 = 0.31\ n_0$$

Using conservation laws for energy, momentum, and mass we obtain the recoil momentum, P, acting on the metal (kg m/sec) as below

$$\frac{P}{Q} = \frac{1.69}{\sqrt{L}}\frac{b}{1+2.2b^2} \qquad (2.19)$$

where Q is energy absorbed by the metal (J), $b^2 = kT_0/mL$, and L is the heat of vaporization per unit mass (J/kg) (Reference 7).

Equation (2.19) provides information on the shock wave. There are three disadvantages of this formula. The first is that it ignores the existence of atmosphere which can cool down the hot vapor immediately after the Knudsen layer. The second is that it ignores the effect of the absorption coefficient α. In other words, it needs revision when the absorption depth of metal is not shallow or atmosphere does exist. The third, which is the vital disadvantage of this formula, is that a shock wave can be generated by vapor explosion which is not taken into account by this formula.

2.4.4 Film-Thickness Temperature Profile

Equation 2.19 also ignores a significant amount of energy being transferred into thermal energy. Such thermal energy is initially highly localized. The heat conduction is based on the assumption that the heat flux, ϕ in J/m^3s, across a plane is proportional to the local temperature gradient

$$\phi(z_0) = -K\,(dT/dz)_{z_0} \qquad (2.20)$$

where K is the thermal conductivity in units of W/m K.

Consider energy balance within a slab of material extending from z to z+dz. The difference between heat entering and leaving in a time dt leads to a rise in temperature, dT, given by

$$dt\,[\,\phi\,(z) - \phi\,(z + dz)\,] = dT\,(\rho\, c_p)\,dz \qquad (2.21)$$

where ρ is the density of material and c_p is its specific heat capacity. Assuming K is a constant, and putting equation 2.20 into 2.21, we derive

$$K\frac{d^2}{dz^2}T = \rho c_p \frac{dT}{dt} \qquad (2.22)$$

To simplify our discussion, assume the photonic distribution in the xy plane is uniform. Thus the initial absorbed energy profile Q(z,t) only changes along z axis and can be expressed as

$$Q = I_0(t)(1- R)\,\alpha\, e^{-\alpha z} \qquad (2.23)$$

where $I_0(t)$ is the input power density of laser beam (J/cm^2), α is absorption coefficient, and R is reflectivity: the unit of Q is J/cm^3.

The temperature profile can be derived if we know the diffusion coefficient, D, in m^2/s, from

$$\frac{dT}{dt} = \frac{Q}{\rho c_p} + D\frac{d^2T}{dz^2} \qquad (2.24)$$

The solution of equation 2.24 is:

$$\begin{aligned} T(z,t) = &[(\frac{2I_0}{K\sqrt{Dt}})\text{ierfc}(\frac{z}{2\sqrt{Dt}}) - (\frac{I_0}{\alpha K})e^{-\alpha z} \\ &+ (\frac{I_0}{2\alpha K})e^{\alpha^2 Dt - \alpha z}\text{erfc}(\alpha\sqrt{Dt} - \frac{z}{2\sqrt{Dt}}) \\ &+ (\frac{I_0}{2\alpha K})e^{\alpha^2 Dt + \alpha z}\text{erfc}(\alpha\sqrt{Dt})](1-R) \end{aligned} \qquad (2.25)$$

When the thermal diffusion length $\sqrt{2Dt}$ is much larger than the optical absorption length $1/\alpha$,which is true for metals, the surface becomes the heat source for the internal material. Only the first term in equation 2.25 is meaningful, thus T can be expressed as:

$$T(z,t) = \left[\frac{2I_0}{K\sqrt{Dt}}\text{ierfc}(\frac{z}{2\sqrt{Dt}})\right](1-R) \qquad (2.26)$$

A typical profile of integral of error function is shown in Figure 2.5 .

The temperature at the interface thus can be determined by letting z in equation 2.26 equal the thickness of the thin film and putting (1-R) = 1. The temperature at the surface of thin film can also be calculated by putting z = 0 and (1 - R) = 1 which finally yields

$$T_0 = \frac{2I_0}{K\sqrt{Dt}} \qquad (2.27)$$

The main disadvantage of this equation is that it assumes the cross sectional distributions along x,y axes are uniform which is not true in our lab.

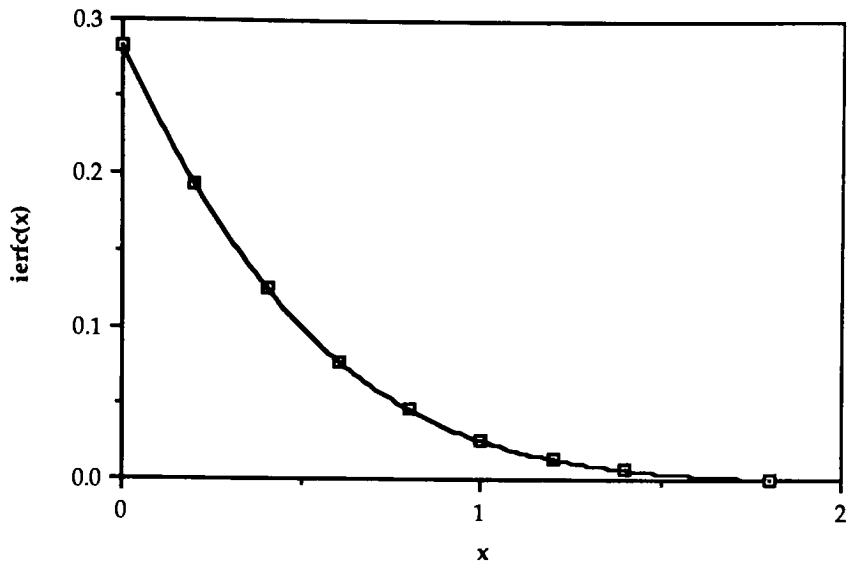

Figure 2.5 A typical profile of integral of error function.

The polymer at the interface can be either solid or liquid which is dependent upon the thermal energy being diffused from metallic thin film. Because of the large deviation of linear thermal expansion coefficients (TEC) of metal and polymer (TEC of silver = 18μm/m°C, TEC of PET = 38 μm/m°C), there will be a strong tensile thermal stress at the interface. Such a thermal stress is one of the major source that initiates cracks on thin film. Fig 2.8 shows this mechanism schematically.

2.5 Subsequent mechanical effect

2.5.1 Overview of the subsequent effects

According to our observations, when the energy density of laser light exceeded a threshold value, the metallic thin film was cracked. Such a threshold energy density was found readily affected by the adhesion (the results are in section 4). We explain this by saying that upon the initiation of a crack, the shock wave has to overcome the adhering attraction at the interface. Fig . 2.6 shows this mechanism schematically. In this research, our observation of all the cracked samples shows that polymer substrate melts

after laser illumination. Hence the adhesion we evaluate is a solid to liquid adhesion. A photograph of the molten layer is in Figure 4.2 .

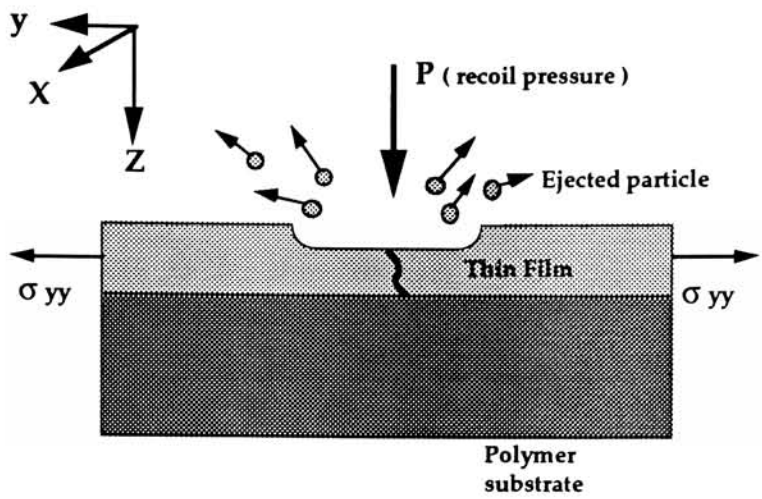

Figure 2.6 A crack is initiated by recoil pressure.

In the following paragraphs, we characterize the relationship between the converted tensile stress (σ_{yy} in Figure 2.6) and the recoil pressure (P in Figure 2.6).We then build a crack initiating model by putting Griffith theory (see section 2.5.2) and the adhesion of liquid layer (see Section 2.5.3) into account.

2.5.2 The tensile stress caused by recoil pressure

As Figure 2.6 shows, the recoil pressure ejects the molten materials within laser impinged region so that a cavity is formed. The recoil pressure acting on the wall of the cavity causes a tensile stress, σ_{yy}, (with regard to the bottom point of the cavity) to form on the thin film.

Because only superheated material can be ejected from the thin film, the shape of the cavity is close to an isothermal plane at which the temperature is equal to the melting point of the metallic thin film. The mechanical effect on the contour of the cavity is thought to be trivial compared to the temperature effect, hence it is neglected in this thesis research. So we suppose the shape and depth of the cavity is determined by the temperature profile. In

other words, it is determined by the distribution of photons of the laser beam and the heat conduction of the material, but not the recoil pressure.

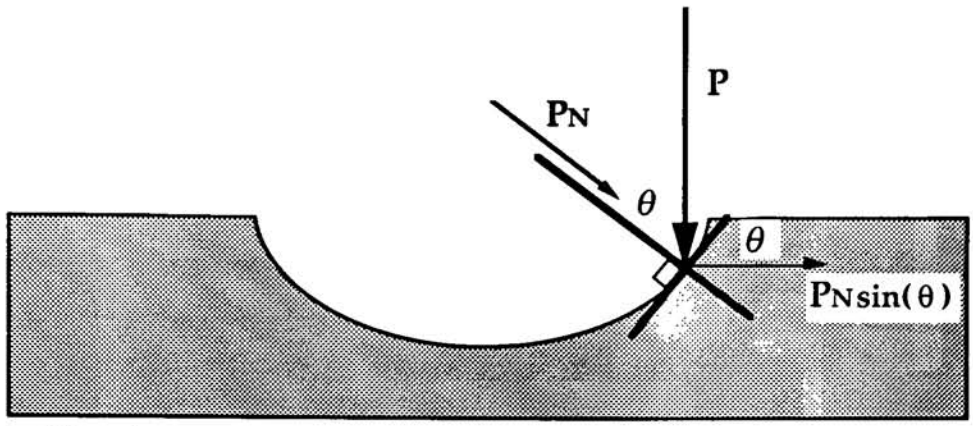

Figure 2. 7 In a laser impinged cavity, a tensile stress ($P_N \cos\theta$) is formed by the recoil pressure P. P_N is the normal stress at a specific point in this figure.

The following analysis shows that the converted tensile stress is proportional to the recoil pressure for a typical cavity. Figure 2.7 shows a cavity being impacted by a recoil pressure P at one point. If the angle between the impact pressure and the normal line of the surface is θ, then the normal stress on thin film, P_N, is equal to $P \cos(\theta)$. Hence the horizontal stress within the material is $P_N \sin(\theta) = P \sin(2\theta)/2$. Integration of the stress along one side of the curvature of the cavity yields the total tensile stress (σ_{yy}). Since the recoil pressure is independent of the curvature of the cavity (our basic assumption), such an integration yields two independent parts, the pressure one and the curvature one. The equation 2.28 shows this reasoning. As the equation 2.28 shows, the converted tensile stress is proportional to the recoil pressure P. Although it is roughly derived, the results of this calculation imply that a simple proportional relationship between the recoil pressure and converted tensile stress is plausible.

$$\sigma_{yy} = k P \qquad (2.28)$$

k is a shape factor which is only dependent on the contour of the cavity.

2.5.3 The tensile stress caused by vapor explosion

As has been mentioned in section 2.4.2, the stress on thin film can also be generated by vapor explosion. Because the same isothermal plane still exists in the vapor explosion mechanism, a similar relationship between σ_{yy} and the pressure caused by explosion is still valid. Hence the horizontal stress σ_{yy} has to take this resource into account, as expressed below:

$$\sigma_{yy} = k\,(P_r + P_e) \tag{2.29}$$

where k is shape factor, P_r is the pressure caused by recoiled particles, and P_e is the pressure caused by vapor explosion.

2.5.4 The thermal stress

Because the difference in the thermal expansion coefficient between metal and polymer is very large, a thermal stress is formed in thin film after laser irradiation. Figure 2.8 shows this mechanism schematically. Thus the horizontal stress σ_{yy} is composed of three items, as expressed below:

$$\sigma_{yy} = k\,(P_r + P_e) + \sigma_t \tag{2.30}$$

where σ_t is thermal stress in the vicinity of the crack.

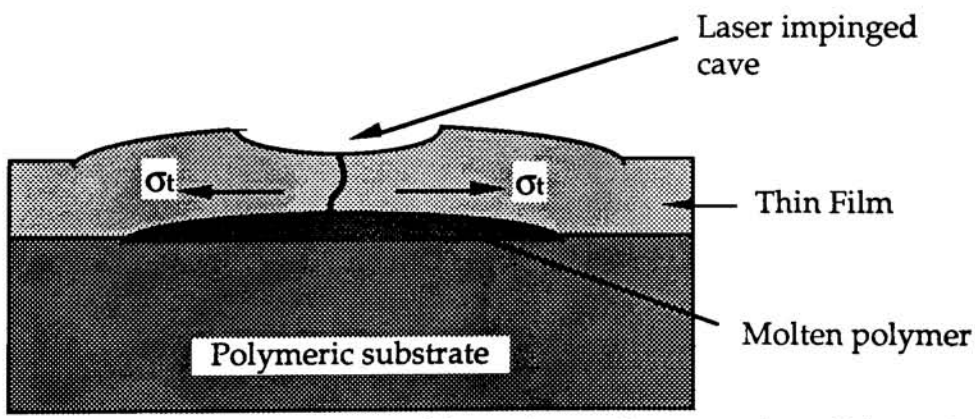

Figure 2.8 Thermal stress caused by volumetric expansion of the polymer.

2.5.5 Griffith crack mechanism on thin films

It is known that a thin film is composed of many columnar grains at the interface (Figure 2.9). The boundaries of these columnar grains serve as the sites of stress concentration as well as the starting point of cracking propagation. Therefore, we deem these boundaries as microcracks within the thin film. From Griffith theory, for a material having a microcrack like Figure 2.10, the fracture strength (σ_f) can be expressed as

$$\sigma_f = \sqrt{\frac{\gamma_{ss} E}{4c}(\frac{\rho}{a})} \qquad (2.31)$$

where γ_{ss} is the surface tension of solid thin film, E is Young's Modulus, 2c is the length of microcrack, a is the mean interatomic distance of thin film, and ρ is the curvature at the tip of microcrack.

Based on this understanding, we know that the minimum net stress required to crack a thin film is σ_f .

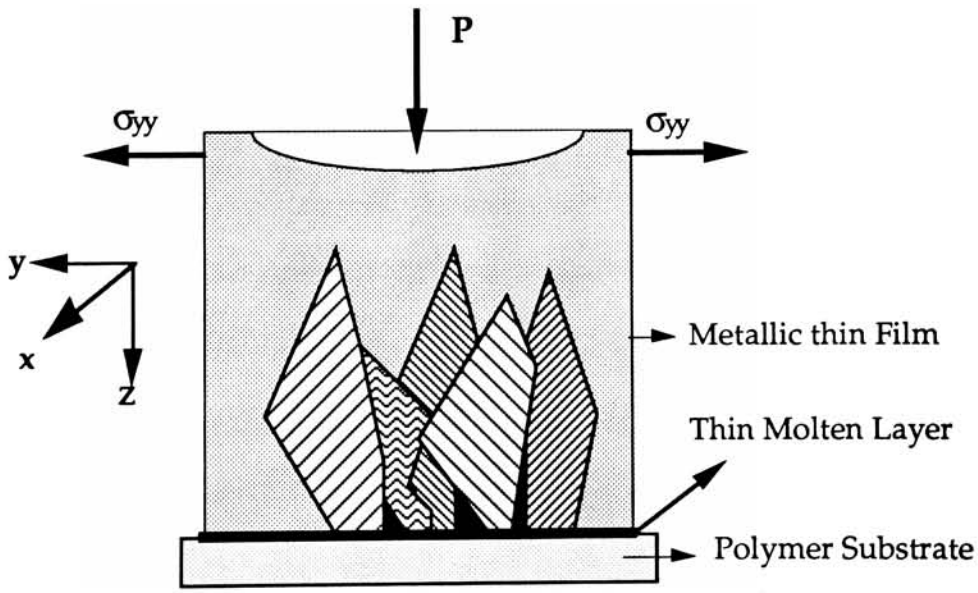

Figure 2.9 Crack is initiated from microcracks.

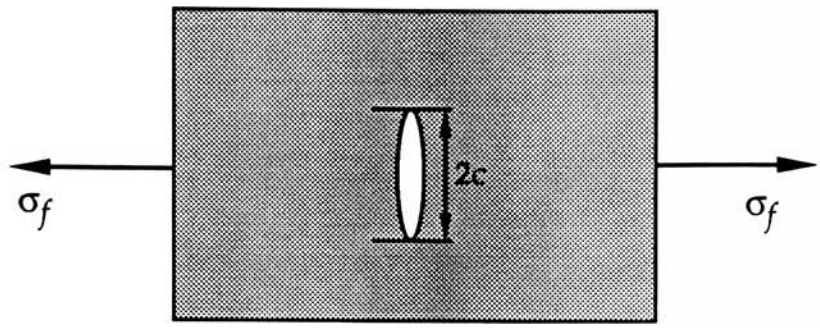

Figure 2.10 A Griffith crack mechanism.

2.5.6 Effect of molten polymer layer on failure mechanism

As has been mentioned in Section 2.5.1, we observed a molten layer of polymer in our laser ablation test. When the polymer is molten, due to strong coupling of thermal and mechanical fields, the metallic thin film still sticks on the viscous polymeric surface by surface tension. As Figure 2.11 shows, a strong surface tension (γ_{sl}, unit: J/m^2) between thin film and molten polymer holds the thin film and polymer together (Reference 1). The minimum stress, σ_a, required to remove the thin film from liquid layer is related to adhesion condition and is determined by surface tension, γ_{sl}, and thickness of liquid layer, h, as

$$\sigma_a = 2\,\gamma_{sl}/h \qquad (2.32)$$

Due to strong capillary attraction at the interstitial between the columns, the molten polymer will fill up the interstitials. This mechanism is shown in Figure 2.12.

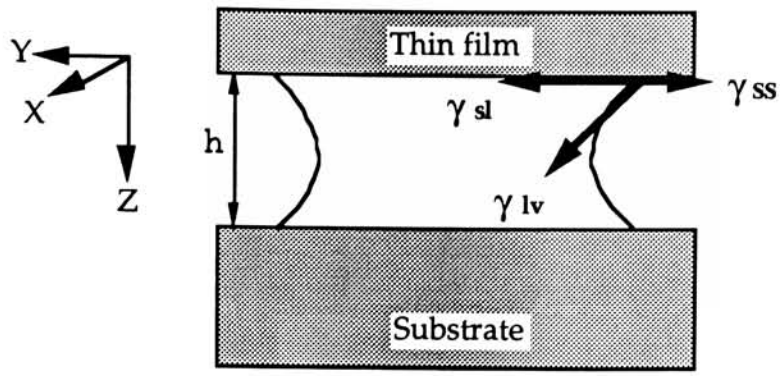

Figure 2.11 Capillary attraction between film and substrate. Subscript s refers to solid, l refers to liquid, and v refers to vacuum.

Of the numerous filled microcracks, consider the one that initiates the propagation of the crack. Figure 2.13 shows an exaggerated interstitial within the thin film. As is depicted by this figure, the tensile stress (σ_{yy}) needs to overcome the adhesion (σ_a) before causing a crack.

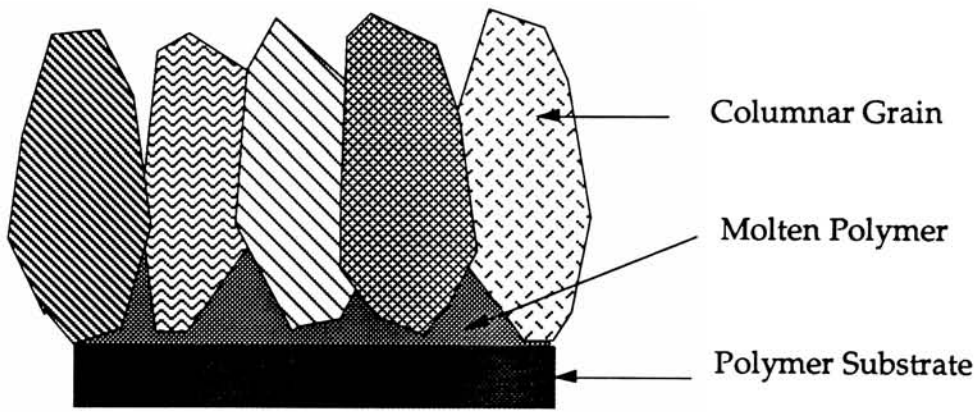

Figure 2. 12 A schematic explanation of the mechanism that the boundaries between the columns at the interface are filled up with the molten polymer.

Therefore, when a crack is about to be initiated, the net horizontal stress, $\sigma_{yy} - \sigma_a$, is equal to fracture strength as is shown below.

$$\sigma_{yy} - \sigma_a = \sigma_f = \sqrt{\frac{\gamma_{ss} E}{4c}\left(\frac{\rho}{a}\right)} \qquad (2.33)$$

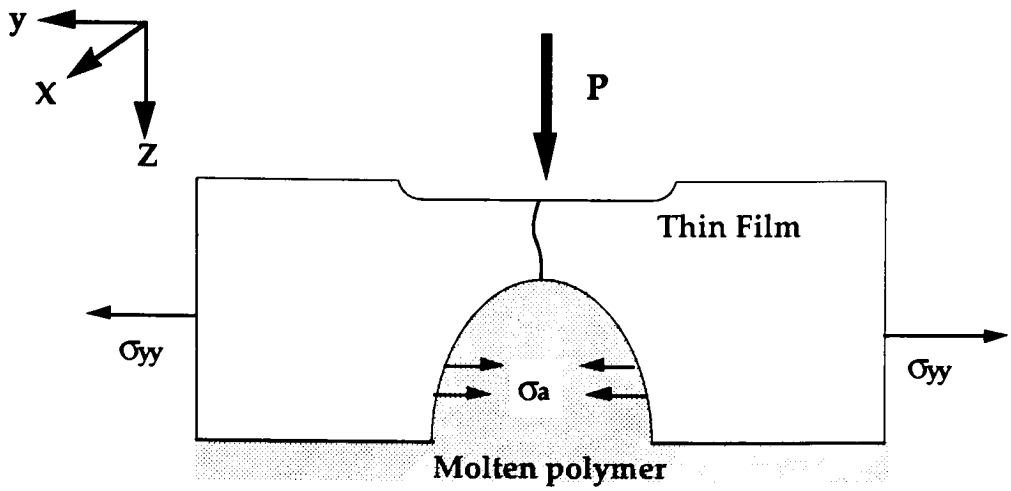

Figure 2.13 Modified Griffith crack mechanism by molten polymer.

Suppose σ_f is a constant for the samples made by the same deposition rate and substrate temperature (thus $d\sigma_f = 0$). We have

$$d\sigma_f = d(\sigma_{yy} - \sigma_a) = 0 \qquad (2.34)$$

$$d\sigma_{yy} = d\sigma_a \qquad (2.35)$$

$$= d(k(P_r + P_e) + \sigma_t) \qquad \text{(from Equation 2.30)}$$

which means that the deviation of tensile stress ($d\sigma_{yy}$) required to crack the thin film is proportional to $d\sigma_a$. Moreover, we can see that σ_a arises from basic adhesion and σ_f measures practical adhesion. So we have virtually separated the contribution of these two mechanisms. Because the three sources of generating tensile stress (P_r, P_e, and σ_t) are all caused by laser illumination, we can change the magnitude of tensile stress by changing the incident energy density of laser light.

3. Experimental Details

3.1 The Laser and the adhesion test

Figures 3.1 and 3.2 show the instrumental installation and the shape of laser beam. The light source is a 401XR excimer laser generator made by Tachisto Incorporated. The laser cavity is charged with HCl at 80 Torr, Xe at 50 Torr, Ne at 1000 Torr, and He at 1470 Torr (Ne and He serve as the buffers for discharge). An electrical discharge of 40 kV initiates the UV laser pulse of about 20 ns duration with wavelength of 308 nm.

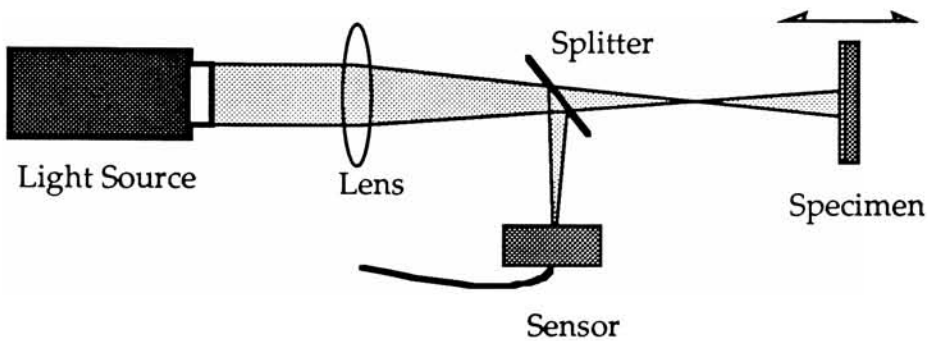

Figure 3.1 Laboratory installation of laser ablation test.

The designed maximum output energy of the gas mixture in our instrument is 400 mJ, but the actual output energy varies due to the nature of excimer. For this reason we monitor the energy of each laser shot by a sensor. The cross section of the output beam is a rectangle, 12 x 25 mm. At the exit of aperture, the beam divergence is 2x6 mrad which is of negligible importance here. We assume therefore that the laser beam continues as a rectangle of length to width 25:12 even as the light is focused by the lens.

Detailed instrumental data are attached in the Appendix on Laser Characteristics.

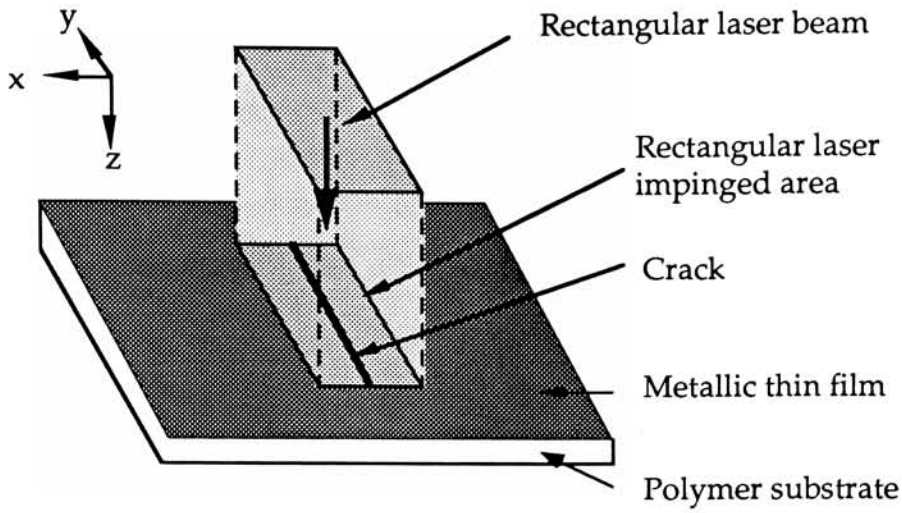

Figure 3.2 The shape of laser beam and the impinged area.

The manufacturer provided the typical profile of laser pulse shown in Figure 3.3. Whenever such a pulse is generated, it then is focused by a quartz lens of nominal focal length 30 cm. Another quartz plate is interposed between the lens and specimen to split a small fraction of the pulse to a sensor made by Molectron Detector Inc., Model J25, Serial # 523. The output energy of the sensor is viewed by an digital oscilloscope (Tektronics 7854) which integrates the output voltage from the sensor to give the energy of pulse.

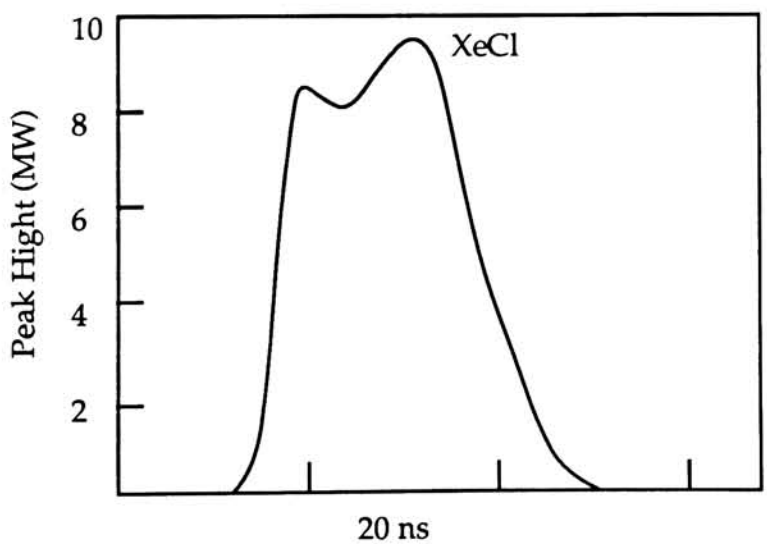

Figure 3.3 Manufacturer provided profile of XeCl Laser.

On the screen of oscilloscope, the pulse is presented as Figure 3.4 (b). The energy density distributions along the x and y axes are shown schematically in Figure 3.4 (c) and (d).

The sensor is designed to give 8 V/J for 337 nm light. When we are doing the test, the lens, splitter, light source, and sensor are immobile. The specimen is held on a stage which always keeps it perpendicular to the laser beam. The position of the stage can be adjusted along three orthogonal axes by micrometers. By moving the specimen closer to the focal point of the lens, we decrease the area of the beam and thus increase the energy density.

Subsequently the samples are viewed under microscope and the results are compared with those of tape tests.

After laser illumination, discoloration and a shallow cavity in the impinged area are visible to the naked eye. When the specimen is moved close enough to the source, a crack is initiated on the film, and the lowest energy density where the crack was initiated is called the threshold energy density.

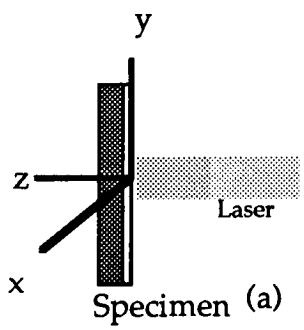

(a)

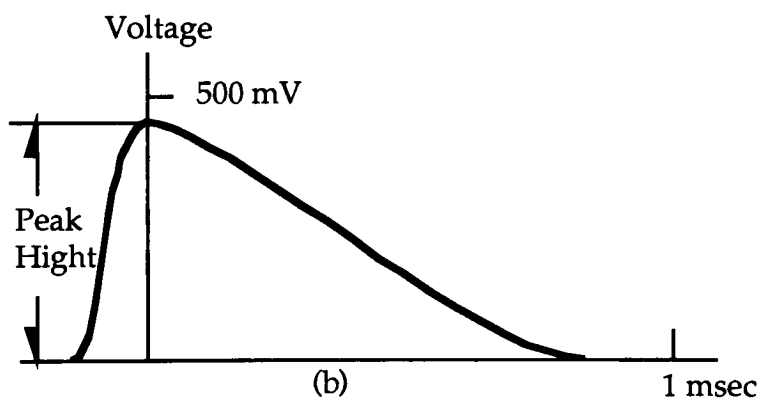

(b)

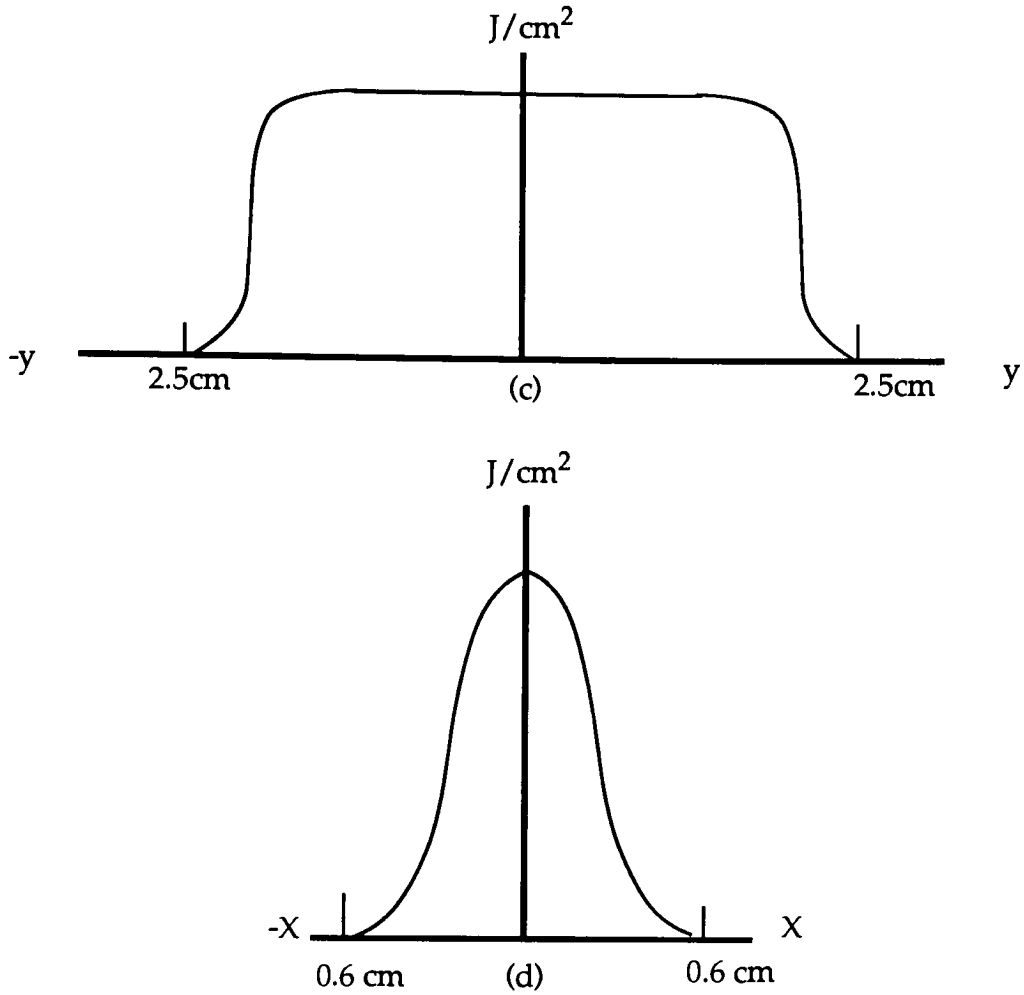

Figure 3.4 A Typical pulse profile. (a) coordinate system. (b) a pulse seen on oscilloscope (c) energy distribution along X axis. (d) distribution along Y axis.

3.2 Determination of incident intensity

As was mentioned in section 3.1, we actually measured the energy of the split beam, E_S, and the distance between lens and target, z. Suppose the splitting ratio is S (Intensity of split beam/Intensity of total flux), then the total energy impinged on the film, E_t , can be written as

$$E_t = A\,(1\text{-}S)\,E_S / S \approx A\,E_S / S \qquad (3.1)$$

where A is the absorbance in decimal scale. Since we control the angle of splitter to make S << 1, (S = 0.0197 in our labs), 1 - S ≈1.

We really wish to know the overall energy density impinged on the sample, and to calculate this we need to know the area of the partially focussed beam. This was done by exposing Kodak photograph paper to laser light and measuring the scorched area.

Because the distribution of laser beam within a region of x axis is uniform (See Figure 3.4), and beyond this region the intensity of the beam is virtually zero, we use a step function to approximate such a distribution. At the edges, the scorched area has a very clear boundary. It is this characteristic, the sharp boundary, that provides us with the accuracy for measuring the laser impinged area. We assume the beam shape is not distorted (length : width = 25 : 12). If the length of laser impinged area is L, the beam area is 0.48 L^2. The length was measured with steel ruler to an accuracy ± 1 mm.

As we change the distance between sample and lens along the z axis, the length of laser impinged area changes according to the following linear relationship

$$L = M z + L_0 \qquad (3.2)$$

where L and L_0 are the length of laser impinged area at position z and focus, M is a linear proportionality, and z is the distance between sample and lens. Figure 3.5 shows this relationship.

Linear regression functions of the two sets of data in Figure 3.5 are

$$y = 3.673 - 0.0979x \qquad x < 27 \text{ cm};$$
$$y = -2.2839 + 0.0876x \qquad x > 27 \text{ cm}.$$

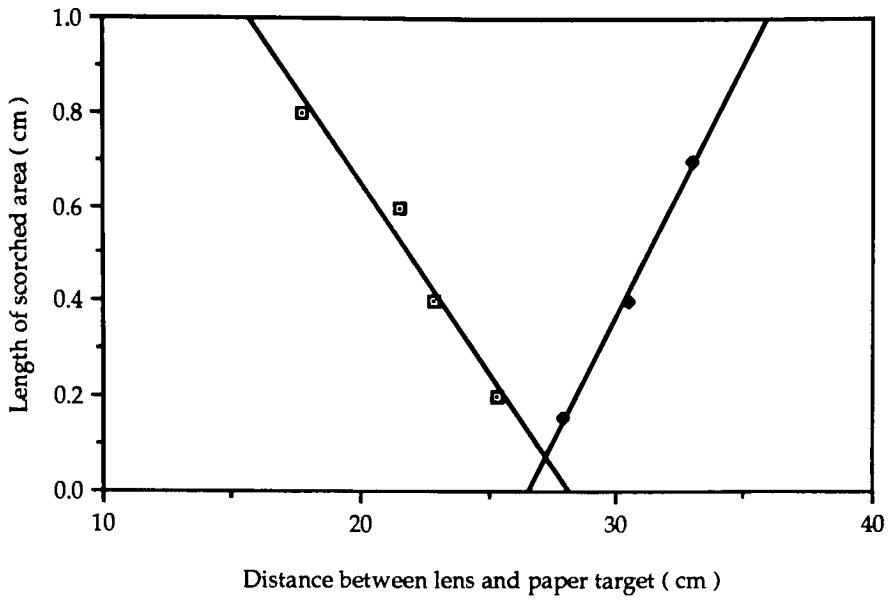

Figure 3.5 Length of laser scorched area of KODAK photograph paper. Vertical axis is the length of the laser scorched area along X axis.

Because we always put our sample farther than the focal length, the line for $x > 27$ is applied. M and L_0 thus are 0.0876 and -3.2839. The negative value of L_0 prohibits us from correctly calculating the length as we push our sample close to the focus. Fortunately, in our test there is no need to place the sample so close to the focus.

The measured focal length of the lens in this test is 27 cm, about 3 cm shorter than the nominal focal length. This because the nominal focal length for the quartz lens is only measured by visible light, not UV light.

For a sample which is placed $z > 30$ cm far away from the lens, the general expression of laser impinged area, Æ, is

$$Æ = 0.48\,(M\,z + L_0)^2. \qquad (3.3)$$

The laser impinged energy density thus can be expressed as

$$I_t = E_t / Æ = A\,E_s / S\,Æ = A\,E_s / (S\,(0.48\,(M\,z + L_0)^2))$$

where I_t is the incident energy density (J/cm^2) absorbed by the thin film and the other parameters are defined as before.

3.3 Sample Preparation

In this thesis research we divided the samples into five groups. The following paragraphs describe the characteristics of each group.

Group 1

In this group silver thin films (6500 Å) were coated on various brands of PET substrates. The PET substrates were made by different manufacturers and have different adhesion properties with respect to silver thin films. They are Dupont 700D 7mil, Kodak Estar 48', Host Hostaphan, and ICI Melinex. The coating process was done by electron-beam deposition at a deposition rate of 360- 430 Å/sec and a pressure between 5×10^{-5} and 5×10^{-4} Torr. A brief description is listed in Table 3.1.

Table 3.1 Characteristics of group 1.

Objective: Characterize the deviation caused by various substrates	
Sample #	Substrate
1	Dupont 700D
2	Kodak Estar 48'
3	Host Hostaphan
4	ICI Melinex
Deposition Rate: 430 Å/sec Ag Thickness: 6500 Å	Base Pressure: 5E-5 ~ 5E-4 T No Glow Treatment

Group 2

In this group silver thin films (4100 Å) were coated on the same PET substrates, Dupont Mylar 4 mil. One of the substrates was processed by oxygen

glow discharge before thin film deposition while the other was not. According to former researcher's records, the surface energy of PET treated by low pressure (0.2 ~ 2.0 torr) oxygen or nitrogen plasma increased from 41 dynes/cm^2 to 73 dynes/cm^2. (Reference 8) We looked to see if this adhesion enhancement by glow discharge could be characterized by the laser ablation test.

The mechanism of polymer surface treatment by a cold gas plasma is depicted in Figure 3.6. By means of an alternating current process, the gas is excited into an energetic state containing many different species and metastables (excited species in transition state), that react with and modify the polymeric substrate. As the excited species and metastables return to lower energy states, they undergo glow-discharge, emitting light that can further modify the substrate as ultraviolet radiation.

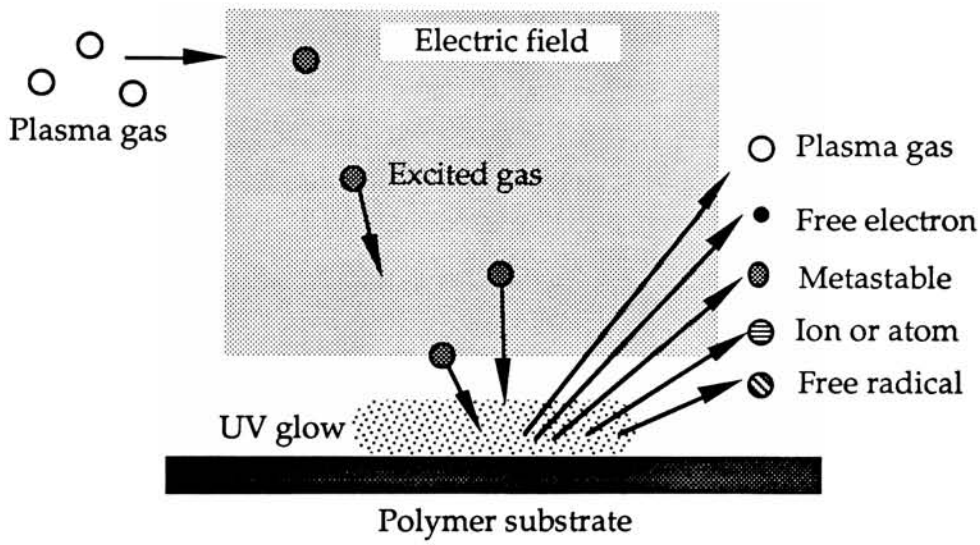

Figure 3.6 A representation of the mechanism of glow discharge.

The glow discharge plasma rapidly modifies the surface of polymer by introducing free radicals. These free radicals increase the molecular attraction of the surface, and thus increase the surface energy or adhesion. (See section 2.5.3 for the relation between surface energy and adhesion.) From a more detailed view, the process of free radical creation by oxygen gas plasma on polymer surfaces has four major effects:

1. Surface cleaning — removing surface containmanents;
2. Ablation — removing weakly bound components;
3. Surface activation — increasing the surface energy by forming polar functional groups;
4. Mechanical Interlocking — increasing the surface roughness.

The third effect, surface activation, definitely increases the bulk bonding energy. Thus it is desirable for adhesion promotion. In addition, once a highly activated polymeric substrate is formed by cold plasma treatment, the deposited atoms or clusters will be drawn into microcracks or voids near the surface of substrate, promoting mechanical interlocking. This also increases the practical adhesion.

In our research, the pressure in the oxygen glow was 20 mtorr. The coating process was done by e-beam deposition at a deposition rate of 430 Å/sec. A brief description is listed in Table 3.2.

Table 3.2 Characteristics of group 2.

Objective: Characterize the deviation caused by glow discharge treatment	
Sample #	Glow Treatment
1	No
2	Yes (Presure of glow =20 mT)
Deposition Rate: 430 Å/sec System: Ag 4100 Å/Mylar 4mil	Base Pressure: 5E-5 ~ 5E-4 T

Group 3.

In this test, we know that samples were glow discharge treated at 30 mTorr and 15 mTorr, with one sample untreated. As was stated by Peter Ross (Reference 8), the extremely complexity of gas plasma (oxygen, for instance, produces at least 13 different types of excited species) and the number and nature of the interactions in the plasma system make the specific chemistry of treated surface nearly impossible to predict. What is predictable is that an

oxygen plasma yields functional groups. The optimal plasma treatment for a given system can therefore only be determined through trial and error. We thus utilize the result of this group to predict the optimal process for Ag/ICI Melinex system.

In this group, the deposition rate was 360 Å/sec. Sample 1 was unglowed, sample 2 was treated at a 30 mTorr glow discharge. Sample 3 was treated at a 15 mTorr glow discharge. A brief description is listed in Table 3.3. Results of laser ablation test are to be compared with those of tape tests.

Table 3.3 Characteristics of group 3.

Objective: Guage the effect of glow discharge treatment	
Sample #	Oxygen Glow Treatment
1	No
2	30 mTorr
3	15 mT
System: Ag 4000 Å /Melinex	Deposition Rate: 306 Å/sec Base Pressure: 5E-5 ~ 5E-4 T

Group 4

In this group silver thin films that had different thickness were coated on the same substrates (ICI Melinex). As was mentioned in the theory section, when the optically excited electrons return to stable states, thermal energy is emitted. After a period of thermal diffusion (20 ns in this test), the metal/polymer interface is heated. Because the glass transition temperature of polymer (T_G = 90K) is much lower than the melting point of the metal, the polymeric substrate at the interface can be molten while the metallic thin film at the interface remains solid. For the thicker films the thermal energy diffuses farther before reaching the interface and the interfacial temperature is

lower. This group is designed to characterize how the thickness of thin film affects the results of laser ablation test. The thickness of the samples were 2000 Å, 5000 Å, 10,000 Å, and 40,000 Å. The coating process was e-beam deposition at rates of 50-100 Å/sec. A brief description is listed in Table 3.4.

Table 3.4 Characteristics of group 4.

Objective: Characterize the deviation caused by film thickness	
Sample #	Film Thickness
1	Ag 2,000 Å
2	Ag 5,000 Å
3	Ag 10,000 Å
4	Ag 40,000 Å
Deposition Rate: 50-100 Å/sec Base Pressure: 5E-5 ~ 5E-4 T Substrate : Melinex	

Group 5

In this group copper thin films (4000 and 5000 Å) were coated on a silicon wafer (P type, 1E15 of B, 2 inch diameter). The objective of this test was to characterize the effect of high melting point substrates on laser ablation test. As was mentioned in the theory section, there may be a thin molten layer under the metallic film after laser irradiation. We used Silicon to see how the laser ablation test works when the substrate is not molten. The coating was done by DC magnetron sputtering at a rate of 2.5 Å/sec. Plasma pressure was varied (for one sample is 2 mTorr, for the other is 10 mTorr) in order to generate different residual stress on the the film. We hoped to see if the intrinsic stress would affect the results of the laser ablation test.

4. Results & Interpretation

4.1 Result of each group

Generally speaking, the threshold energy density of the laser ablation test correlates well with the tape test. In all cases, the error range of laser ablation test is 10 mJ/cm^2 and that of tape test is 10%. In all groups, the threshold value is the estimated energy density that can initiate cracks on thin films. Notice that the data EL in all tables are refered to the highest measured energy densities which do not initiate cracks on the thin films. The data EU are referred to the lowest measured energy density which initiates a crack on the thin film. Thus the deviation between EL and EU gives the ranges of accuracy for each measurement.

GROUP 1 **Silver on different PETs**

The objective of this group was to characterize the variation in adhesion caused by different brands of PET substrates. Results are listed in Table 4.1. Uncertainties in measuring the area lead to an uncertainty in energy density of $\pm$ 10 mJ/cm^2. In the tape test, the fraction of the coating that is removed is estimated visually to an accuracy of about 0.10.

Both tests suggest that Ag/Dupont 700 D 7mil has the worst adhesion and Ag/ICI Melinex has the best. Results differ for tests of Ag/Kodak Estar 48' and Ag/Host Hostaphan. The laser ablation test suggests that Ag/Kodak Estar 48' (43 $\pm$ 10 mJ/cm^2) and Ag/Host Hostaphan (46 $\pm$ 10 mJ/cm^2) have similar adhesion while the tape test suggests that adhesion is different (0.40 $\pm$ 0.10 compared to 0.60 $\pm$0.10). Further study is required to clarify the differences.

Table 4.1 Results of group 1.

Objective: Characterize adhesion between silver and different PET substrates					
Sample #	Substrate	Laser Energy Density ± 10 mJ/cm²			Scotch Magic Tape Test Amount Removed ± 0.1
		E_L	Threshold	E_U	
1	Dupont 700D 7 mil	12	13	13	0.90
2	Kodak Estar 48'	38	43	46	0.40
3	Host Hostaphan	45	46	50	0.60
4	ICI Melinex	53	54	57	0.10

Film: Ag 6500 Å — Deposition pressure: 5E-5~5E-4 Torr

Deposition Rate: 430 Å/sec — No glow treatment

E_U: Maximun energy density that does not break the film.

E_L: Minimum energy density that does not over-damage the film.

GROUP 2 Effect of glow discharge on adhesion

The objective of this group was to characterize the effect of glow discharge on the adhesion of the systems. Data are listed in Table 4.2.

For untreated PET, adhesion was poor, 18 mJ/cm^2 and 95% removal, while glow discharge treated samples yielded good adhesion, 125 mJ/cm^2 and 5% removal. Therefore, both tests gave a similar conclusion: adhesion of silver to treated PET is superior to adhesion of silver to untreated PET. This is consistent with our knowledge about glow discharge. (see Figure 3.6)

Table 4.2 Results of group 2.

Objective: Characterize the deviation caused by glow discharge treatment					
Sample #	Glow Discharge	Laser Energy Density ± 10 mJ/cm²			Scotch Magic Tape Test Amount Removed ±0.10
		E_L	Threshold	E_U	
1	No	17	18	19	0.95
2	Yes	122	125	127	0.05

System: Ag 4100 Å/Mylar 4mil Base pressure: 5E-5~5E-4 Torr

Deposition Rate: 430 Å/sec Pressure in glow = 20 mTorr

E_U: Maximun energy density that does not break the film.

E_L: Minimum energy density that does not over-damage the film.

GROUP 3 Effect of different glow conditions

In this test, samples were treated at different levels of glow discharge and the adhesion of silver to the samples were compared. Results are listed in Table 4.3.

Both the laser ablation test and the tape test suggest that the best process is glow at 15 mTorr and the worst process is no glow. But the resolution on the deviation is much different between the two tests. The tape test does not show significant differences between the three conditions while laser ablation test does. The reason why the treatment at 30 mTorr gives lower threshold than that at 15 mTorr needs further study.

Results of this group also can only be compared with the same ones in the other groups in a relative sense. The reason is that we realigned the beam and readjusted the splitter. The new splitting ratio was not measured. Hence the energy densities are not known in an absolute sense.

Table 4.3 Results of group 3.

Objective: Characterize the effect of glow discharge					
Sample #	Glow Discharge	Laser Energy Density ± 10 mJ/cm²			Scotch Magic Tape Test Amount Removed ± 0.10
		E_L	Threshold	E_U	
1	No	368	383	398	0.99
2	15 mTorr	537	540	543	0.90
3	30	404	412	416	0.94

System: Ag 6500 Å/Melinex Deposition pressure: 5E-5~5E-4 Torr
Deposition Rate: 306 Å/sec
E_U: Maximun energy density that does not break the film.
E_L: Minimum energy density that does not over-damage the film.

Generally speaking, in this group the laser ablation test does show advantages over the tape test by its sensitivity to the small changes in adhesion. The tape test can only measure adhesion as a fraction between 0 and 1 with an uncertainty of 0.10. Thus only ten levels are available. In this respect, laser ablation test is much better in that it has a wider range to quantify the adhesion property.

GROUP 4 Effect of thickness

The objective of this group was to characterize the effect of film thickness on adhesion test. Previous work (Section 2.1) suggested that the main effect of laser irradiation on a metallic film is thermal, and that to generate thermal stress large enough to break the film the temperature at interface should exceed a certain value, which means the result of laser ablation test is affected by the thickness of the film readily. We were to check if this is true in our test. Results are listed in Table 4.4.

Table 4.4 Result of group 4.

Objective: Characterize adhesion between silver and different PET substrates					
Sample #	Thickness	Laser Energy Density ± 10 mJ/cm²			Scotch Magic Tape Test Amount Removed ± 0.1
		E_L	Threshold	E_U	
1	2,000 Å	12	13	13	0.0
2	5,000 Å	22	23	24	0.40
3	10,000 Å	45	47*	47	0.60
4	40,000 Å	no threshold reached			0.10
Film: Ag 6500 Å Deposition Rate: 430 Å/sec E_U: Maximun energy density that does not break the film. E_L: Minimum energy density that does not over-damage the film.				Base pressure: 5E-5~5E-4 Torr No glow treatment	

* Crack is not clearly visible.

According to the results of the laser ablation test, threshold energy density increases as the thickness of the film increases. When the film is 40,000 Å thick, no threshold of damage could be reached. Therefore, the estimated energy density required to break the thin film is more than 57 mJ/cm^2. On the other hand, the result of tape test shows that adhesion decreases as the thickness of films increases. The seeming contradiction can be resolved by taking thermal diffusion into account. As mentioned earlier (see Section 2.4.2), a simplified model of temperature profile provided an estimate of a one-dimensional thermal diffusion length of 20 Å. Assuming that the three dimensional length is similar we should expect the thermal energy to diffuse away from the laser-irradiated site, and when the silver became thick enough, the thermal energy reaching the interface should be insufficient to cause adhesion failure.

In addition to insufficient energy being transferred to the interface, another possible effect caused by thick coating is the changing of failure mechanism. Because the heat generated by laser irradiation forms a layer of

molten polymer material at the interface, the adhesion we measured in this thesis research is a solid/liquid adhesion. A thick film thus may prevent enough thermal energy being diffused into the polymer substrate to form such a thin molten layer. Without such a layer of molten polymer, our proposed failure mechanism (see Section 2.5) for solid/liquid adhesion is no longer valid. Thus the required laser energy density for overcoming the adhesion of a solid/solid adhesion system is much higher than it is for a solid/liquid adhesion system. This ideology is expressed schematically in Figure 4.1.

The system we measured in this group, Ag/ICI Melinex, is the same as the sample #4 in group 1, but the adhesion results for the two samples were different. This suggests that some characteristics of Ag/ICI Melinex are different between group 1 and 3. Because of this, inter-group correlation can be only done in a relative sense. The source of variation needs further study.

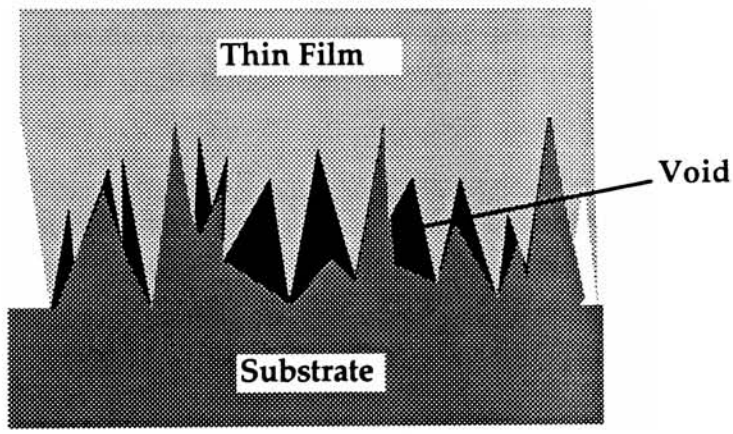

Figure 4.1 A solid/solid adhesion mechanism. Breaking the system requires extra energy compared to liquid/solid system, so a much higher energy density of laser light is required for a solid/solid system than for a liquid/solid system.

GROUP 5 **Copper on silicon**

The objective of this group was to check if the substrate with high melting point (hence no molten layer at the interface) changed the result of laser ablation test. In addition, we wished to discern the effect of residual

stress on the result of laser ablation test. The thin film was not cracked at the moment of laser irradiation but changed into debris a short while later (3 sec or so). A tape test showed that the entire copper film could be detached from silicon wafer very easily. The phenomenon that the film is not broken at the instance of laser irradiation suggests our former crack mechanism is no longer valid here. For these reasons we can not discern the threshold at all. More work is needed to clarify this system.

4.2 Overview of Results

The results of laser ablation test in Group 1, characterization of different brands of substrates, and Group 2, characterization of glow discharge treatment, were generally consistent with the tape test. The only exception was Ag/Kodak Estar which was characterized as fair by laser ablation test (43 $mJ/cm^{2)}$ but poor by tape test (40% off). More work is needed to clarify this. We know that the result of tape test has much wider error range compared to the laser ablation test. The angle of peeling and rate of peeling affect the result readily. In addition, for the tape test, small changes in adhesion are hard to measure, while the laser ablation test has better resolution of small changes.

For a polymeric substrate the laser ablation test leads to melt at the interface. Figure 4.2 is a photograph of a typical crack on the film. We see a wavy structure within the pulled-open groove. This structure is indicative of the melted polymeric layer at the interface. Thomas Bahners and Eckhard Schollmeyer, (Reference 9) observed a simpler structure for polymers directly heated by an excimer laser of sufficient intensity.

Although in our case we have put an Ag film on the substrate to shield direct exposure of the polymeric material, the polymeric material still suffers from severe heating because of high thermal diffusivity of the silver thin film (see Section 2.4). Therefore, it is plausible that our polymeric substrate became molten after the laser irradiation on Ag.

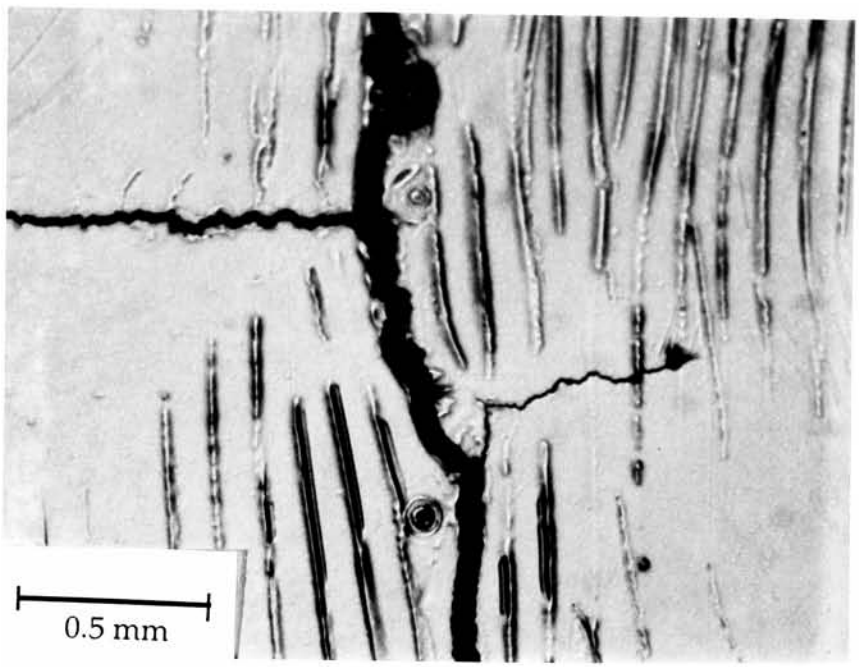

Figure 4.2 A typical structure of laser irradiated area (200X). Wavy structures within the groove are formed by the melted polymeric underlayer. Sample is Ag/Dupont 700 D 7 mil (#1 in group 1). Incident laser energy density is 13 mJ/cm^2.

Another photograph, Figure 4.3, shows that many wrinkles are formed around the crack. Historically, a fine periodic structure on the surface of laser irradiated metals is known to be formed by the electromagnetic field interference of incident laser light and the scattered wave at the surface for a duration of irradiation of a few ms. This might not be applicable in our case because the pulse duration of our laser beam is short (20 ns). Therefore, we suggest they are formed by some other mechanisms.

Figure 4.3 Wrinkles are fromed around the crack (50X). The sample is the same as the one in Figure 4.2.

Figure 4.4 shows a photograph taken by Thomas Bahners' group (Reference 9). As they surmised, the morphology observed is formed by a molten polymer layer (about 0.1 mm thick). Bahners' group also found that for a stressed PET material, there were many rolled structures on PET surface due to Marangoni convection, a type of convection driven by stress field(Reference9). A photograph of such a rolled surface is shown in Figure 4.5. Based on this work, we are convinced that the stressed PET surface may form rolled structures through laser irradiation.

A similar wrinkled surface has been found in our sample (see Figure 4.3). We explain this phenomenon by saying that the molten polymer layer has experienced a compressive stress field during the cooling process. Such a compressive stress could be caused by the volumetric contraction of PET from

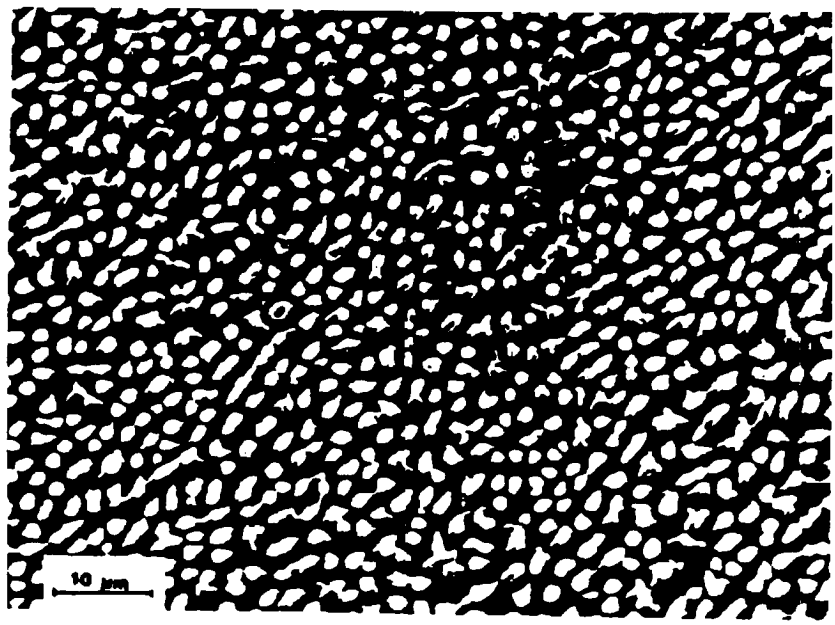

Figure 4.4 A photograph of molten PET formed by excimer laser irradiation (UV 248 nm, 90 mJ/cm^2). After the cooling process, the molten surface coagulates into drizzles due to a strong surface tension (Reference 9)

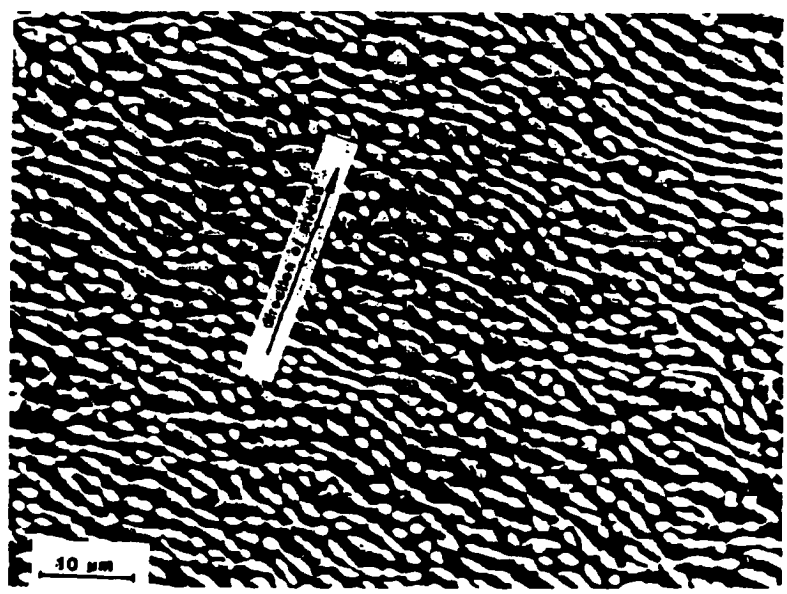

Figure 4.5 A photograph of "roll structure" of stressed PET. Sample was drawn by 10% during laser irradiation. (Reference 9)

liquid to solid phase. A schematic presentation of this mechanism is shown in Figure 4.6.

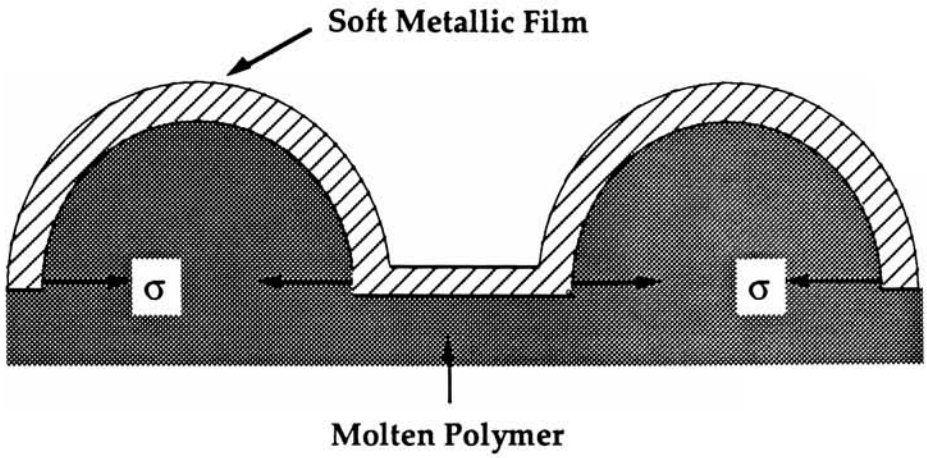

Figure 4.6 The mechanism of wrinkle formation.

5. Conclusion and Recommendation

5.1 Conclusion

This thesis has shown that the laser ablation test does work as an alternative means to measure adhesion. The results presented in this thesis show a correlation between the laser ablation test and the tape test. The laser ablation test has at least two advantages over the tape test: first, it has a broader range of measurement and good sensitivity to small changes in adhesion. Second, its quantitative data is more meaningful as compared to a tape test.

Evaluation of coatings with different thickness cannot be done because the results of the laser ablation test are very thickness dependent. Further work on modelling of the heat flow may remove this problem.

The main drawback of this method is that the light source, an excimer laser, is expensive. In addition, the laser-generated thermal effect plays a critical role so that this method has limitation of only being effective on metallic thin films. No work has yet been done for non-metallic coatings having lower thermal conductivities. If these hindrances can be overcome, laser ablation can serve as a quick, sensitive, and reliable mean to evaluate adhesion.

5.2 Recommendations

Further work to clarify the failure mechanism is still required. There are two ways to approach this objective. First, the thermal stress caused by the volumetric expansion of polymeric substrate can be modeled using numerical analysis. Once the thermal effect caused by laser irradiation is clearly known, we may construct a relationship between the incident energy density and thermal stress quantitatively. Second, a pendulum test can be used to measure the recoil momentum of the sample (References 3, 20). This method directly characterizes the relationship between recoil momentum and

incident energy density. Based on these results, we can re-evaluate or modify the failure mechanism we constructed in this thesis research.

The method of determining the incident energy density also needs improvement. We used a paper burning method to reveal the contour of laser impinged area which ignores the Gaussian profile of the beam along one axis. Further revision is needed to take this into account.

Determination of splitting ratio should be done more carefully. Due to the nature of the excimer laser, the energy of each laser shot varies. In this thesis research we calibrated the splitting ratio by using one thermal sensor to measure the energy of twenty shots, ten unsplit and ten split. In the future, this method should be updated by using two sensors to monitor the split beams simultaneously.

The laser ablation test has also proved effective in measuring thin films on a glass substrate (see section 1.3.1). It is not believed that melting would occur for a glass substrate so the failure mechanism needs more study.

The backside irradiation test, suggested by John Vossen, eliminates the thermal effect on the film/substrate interface. This could be a good way to study the laser ablation test in the future.

6. Appendix The XeCl Excimer Laser

When a rare gas (R) is blended with a halide gas (H), a fraction of the atoms may form a metastable combination (RH)*, the excimer. This unstable combination can be separated by a weak electromagnetic stimulation. As is shown in Figure 6.1, the various stationary quantum states of the electron in the metastable molecule possesses an energy higher than the ground state. Through a stimulated emission process, the electron may return to the stable state with the energy difference being transferred into laser light.

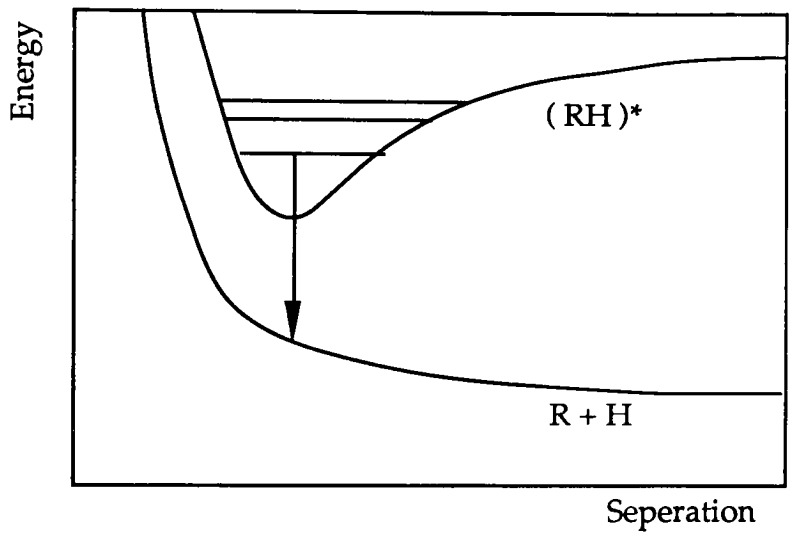

Figure 6.1 Energy vs. atomic separation diagram. R refers to a rare gas atom and H refers to a Halide atom. Using electrical discharge, the unstable (RH)* can be separated, with the extra energy being emitted as ultraviolet light. For the XeCl excimer, the wavelength is 308 nm.

In this thesis experiment, 50 Torr of Xe and 80 Torr of HCl were pumped into the laser cavity. A 40 kV electrical discharge initiated the laser light. Figure 6.2 shows the system of the laser generator.

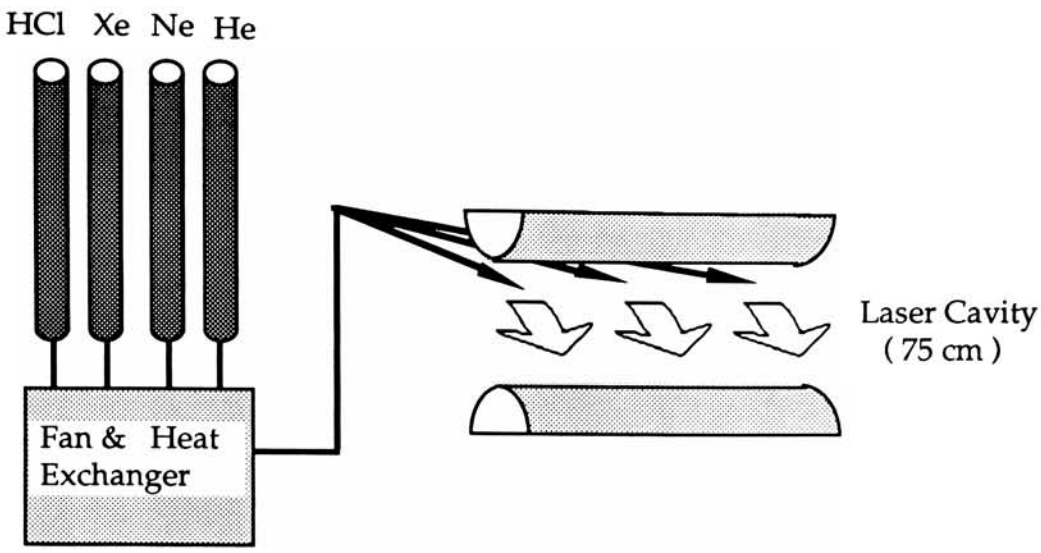

Figure 6.2 Brief view of laser generator. The gas partial pressures were HCl = 80 Torr, Xe = 50 Torr, Ne = 1000 Torr, and He = 1440 Torr. A 40 KV electrical discharge was used to trigger the laser light. Reflector's transmission = 10%.

7. References

1. Mittal, K. L., *Adhesion Measurement: Recent Progress, Un-resolved Problems, and Prospects,* Adhesion Measurement of Thin Films, Thick Films and Bulk Coatings, ASTM STP 640, K. L. Mittal, Ed., American Society for Testing and Materials. 1978, pp. 5-17.

2. Vossen, J. L., *Measurement of Film-Substrate Bond Strength by Laser Spallation,* Adhesion Measurement of Thin Films, Thick Films and Bulk Coatings, ASTM STP 640, K. L. Mittal, Ed., American Society for Testing and Materials. 1987, pp. 122-133.

3. N. C. Anderholm, *Laser-Generated Stress Waves,* pp. 113-115, Applied Physics Letters, Vol.16, No. 3, 1970.

4. P. H. Wojciechowski, F. J. Durate, and A. L. Hrycin, *Excimer laser ablation of metallic thin films: application to adhesion measurement,* Proc. Int'l Conf. on Lasers 1987, F. J. Durate, Ed., STS Press McLean VA (1988) 1097-1104".

5. Martin von Allmen, *Laser-Beam Interactions with Materials,* Chp.1: Introduction; Chp. 2: Absorption of Laser Light; Chp. 3: Melting & Solidification; Chp. 5: Evaporation and Plasma Formation, Springer-Verlag Berlin Heidberg, 1987.

6. Eisberg Robert & Robert Resnick: *Quantum Physics of Atoms, Molecules, and Particles* , Second Edition, pp. 371, John Wiley & Sons Inc.,1985.

7. S. I. Anisimov,*Vaporization of Metal Absorbing Laser Radiation,* pp.182-183, JETP, Vol. 27, No. 1, July 1968.

8. Peter W. Ross and Edward M. Liston,*Treating plastic surfaces with cold gas plasmas,* pp. 41-46, Plastics Engineering, Oct., 1985.

9. Thomas Bahners and Eckhard Schollmeyer, *Morphological changes of the surface structure polymers due to excimer laser irradiation: A synergetic effect?* , Journal of Applied Physics 66(4), 15 August 1989, pp.1884-1886

10. Michell N. F., *Ablation of gallstones using excimer laser pulses,* pp. 2864-2866, Journal of Applied Physics, Vol. 65, No. 7, 1989.

11. X. D. Zhu, *Laser Induced Thermal Deposition of CO on Ni (111) Determination of Pre-exponential Factor and Heat of Desorption,* pp. 459-462, Chemical Physics Letters, Vol.155, No. 4,5, 10, March. 1989.

12. R. J. von Gutfeld, *Electronic probe measurement of pulsed copper ablation at 248 nm*, pp. 1212-1214, Applied Physics Letters, Vol. 54, No. 13, March 27, 1989.

13. I. Ursu, *Pulsed 10 μm-Laser Interferometery of the Early Evolution Stage of a Laser-Generated Breakdown Plasma in Air in Front of an Aluminum Target*, pp. 9-19, Infrared Physics, Vol. 29, No. 1, 1989".

14. Ian W. Boyd, *Laser Processing of Thin Films and Microstructures*, Chp. 2: Interaction and Kinetics; Chp. 6: Material Removal.

15. R. R. Freman, *Behavior of a simple metal under ultrashort pulse high intensity laser illumination*, pp. 159-163, High Intensity Laser-Matter Interactions, Vol. 913.

16. A. D. Bandrauk, S. Chelkowski, *Pulse Instabilities in Molecular Amplifying Media*, pp. 9-16, High-Intensity Laser -Matter Interactions, Vol. 913.

17. B. N. Chapman, *Thin Film Adhesion*, pp. 106-113, Journal of Vacuum Science and Technology, Vol. 16, No.3, 1970.

18. R. Descoste, *Ablative acceleration of laser-irradiated thin foil targets*, pp. 1673-1677, Physical Review Letters, Vol. 42, No. 25, 18 June, 1979.

19. A. Raven, *Stability of Ablatively accelerated thin foils*, pp. 1049-1053, Physical Review Letters, Vol. 47, No. 15, 1981.

20. J. A. Fox, *Laser Induced Stress Waves in 6061-T6 Aluminum*, pp. 2647-2548, Applied Optics, Vol. 12, No. 11, Nov. 1973.

21. N. A. Ebrahim, *Anomalous Energy Transport to Rear Surface of Microdisks at High Laser Irradiance*, pp. 1995-1998, Physical Review Letters, Vol. 43, No. 27, 31 Nov. 1979.

22. B. Arad, *Burn Through Thin Aluminum Foils by Laser-Driven Ablation*, pp. 6817-6821, Journal of Applied Physics, Vol. 50, No. 11, Nov. 1979.

23. A. J. Palmer, "*A study of homogenization and dispersion of laser induced stress waves*",pp. 227-229, "Applied Optics, Vol. 9, No. 1, Jan, 1970".

24. R. Decoste, *Ablative Acceleration of Laser-Irradiated Thin Foil Targets*, pp. 1673-1677, Physical Review Letters, Vol. 42, No. 25, June 1979.

25. M. H. Key, *Study of Ablatively Imploded Spherical Shells*, pp. 1801-1804, Physical Review Letters, Vol. 45, No. 22, Dec. 1979.

26. J. Grun, *Characteristics of Ablation Plasma from Planar Laser Driven Targets*, pp. 545-547, Applied Physics Letters, Vol. 39, No. 7, Oct. 1981.

27. P. A. Steinmann, *A Review of Mechanical Tests for Assessment of Thin-Film Adhesion*, pp. 2267-2272, Journal of Vacuum Science and Technology, A, Vol. 7, No. 3, May/June, 1989.

28. W. Schulz, *Ablation of Opaque Surface Due to Laser Irradiation*, pp. L173-L177,"Applied Physics, Vol. 19, 1986".

29. S. Albin, *Laser Damage Threshold of Diamond Films*, pp. 281-285, Optical Engineering, Vol. 28, No. 3, March 1989.

30. S. A. Metz, *Impulse Loading of Targets by Subnanosecond Laser Pulses*, pp. 211-213. "Applied Physics Letters, Vol. 22, No. 5, March 1973".

31. Domen, K, Chuang T. J., *Laser-Induced Photo-dissociation and Desorption .2. CH_2I_2 Absorbed on Ag*, pp. 3332-3338, "Journal of Chemical Physics, Vol. 90, No. 6, 1989".

32. M. River, *Visualization of Temperature Profiles in a-Si Crystallization in the Explosive Mode by CW Laser*, pp. 185-190, "Laser-Solid Interactions and Transient Thermal Processing of Materials", Materials Research Society, Symposia processing, Vol. 13 .

33. V. I. Igoshin and V. I. Kurochkin, *Laser evaporation of metals in a gaseous atmosphere*, pp. 1049-1052, Sov. J. Quantum Electronics, Vol. 14, No. 8, Aug. 1984.

34. V. I. Mazhukin and A. A. Samokin, *Kinetics of a phase transition during laser evaporation of a metal*, pp. 1608-1611, Sov. J. Quantum Electronics, Vol. 14, No. 12, Dec. 1984.

35. David W. Gregg and Scott J. Thomas, *Momentum transfer produced by focused laser giant pulses*, pp.2787-2789, "J. Applied Physics, Vol. 37, No. 7, June 1966".

36. A. A. Vedenov, O. P. Ivanov, and A. L. Chernyakov, *Theory of laser radiation damage to surfaces of opaque materials*, pp. 1587, Sov. J. Quantum Electronics, Vol. 14, No. 12, Dec. 1984.

37. J. E. Andrew, P. E. Dyer, D. Forster, and P. H. Key, *Direct etching of polymeric materials using XeCl laser*, pp. 717-719, Applied Physics Letters, Vol. 43, No. 8, Oct. 1983.

38. Yong-Kil Kim, Chin-An Chang, and A. G. Schrott, *Adhesion of metals to spin-coated fluorocarbon polymer films*, pp. 251-254, Journal of Applied Physics, Vol. 67, No. 1, January 1990.

39. D. J. Broer and L. Vriens, *Laser-Induced Optical Recording in Thin Films*, pp. 107-123, Applied Physics A, Vol. 32, 1983.

40. G. Charatis, *Simultaneously time- and space- resolved spectroscopic characterization of laser-produced plasma*, pp. 118-123, High Intensity Laser-Matter Interactions, Vol. 913.

41. D. H. Lownes, *Pulsed Excimer Laser (308 nm) Annealing of Ion Implanted Silicon and Solar Cell Fabrication*, pp. 407-412, Laser-Solid Interactions and Transient Thermal Processing of Materials, Materials Research Society, Symposia Proceedings, Vol. 13.

42. Marc L. Sentis, Philipe Delaporte, Bernard M. Foresteir, and Bernard L. Fontaine, *Parametric studies of x-ray preionized discharge XeCl laser at single shot and at high pulse rate frequency (1kHz)*, pp. 1925-1930, Journal of Applied Physics, Vol. 66, No. 5, 1 Sept, 1989.

43. S. G. Hansen, *Study of ultraviolet-laser ablation products of several polymers using time-of-flight mass spectroscopy*, pp.1411-1422, Journal of Applied Physics, Vol. 66, No. 3, 1 Aug., 1989.

44. K. Imen, J. Y. Lin, and S. D. Allen, *Steady-state temperature profiles in thermally thin substrate induced by arbitrarily shaped laser beams*, pp. 488-491, Journal of Applied Physics, Vol. 66, No. 2, 15 July, 1989

45. F. Cottet and M. Boustie, *Spallation studies in aluminum targets using shock wave induced by laser irradiation at various pulse duration*, pp. 4076-4073, Journal of Applied Physics, Vol. 66, No. 9, 1 Nov., 1989.

46. Jovicevic. S., *CO_2 Laser-Induced Plasma Formation on a Copper Surface Covered by Dielectric Particles*, pp. 283-187, Applied Physics, Vol. 48, No. 3, 1989.